The Lindeques Drift and Heidelberg Intrusions and the Roodekraal Complex, Vredefort, South Africa: comagmatic plutonic and volcanic products of a 2055 Ma ferrobasaltic magma

S.A. de Waal
Centre for Research on Magmatic Ore Deposits, Department of Geology, University of Pretoria, Pretoria 0002, South Africa.
e-mail: sybrand@dewaals.com

I.T. Graham
Centre for Research on Magmatic Ore Deposits, Department of Geology, University of Pretoria, Pretoria 0002, South Africa.
Geoscience, Australian Museum, 6 College St, Sydney, NSW 2010, Australia.
e-mail: iang@austmus.gov.au

R.A. Armstrong
PRISE, Research School of Earth Sciences, The Australian National University, Canberra, ACT 0200, Australia.
e-mail: richard.armstrong@anu.edu.au

ABSTRACT

The Lindeques Drift and Heidelberg Intrusions and the volcanic Roodekraal Complex belong to a high-Ti mafic igneous suite (HITIS) that was emplaced in the Kaapvaal Craton as km-sized bodies, to the north and north-east of the Vredefort impact structure, prior to impact. New zircon SHRIMP ages for the Lindeques Drift Intrusion (2054.8 ± 5.7 Ma) and Roodekraal Complex (2053 ± 9.2 Ma) are indistinguishable from that of the Bushveld magmatic event (~2.06 to 2.05 Ga). The dominant rock types in the Lindeques Drift and Heidelberg Intrusions are even-grained and porphyritic spessartites which essentially are clinopyroxene-magnetite (-ilmenite) ± olivine cumulates with variable fractions (estimated 15 to 30%) of interstitially crystallized magma. The concentration of magmatic amphibole (edenite-magnesiohastingsite), responsible for the porphyritic texture of the spessartite, is directly proportional to the fraction of trapped magma, which also crystallized interstitial plagioclase, sphene, sulphide, apatite, microperthite and biotite. The Lindeques Drift spessartite is cut by fine-grained dykes and sills(?) of diorite and syenodiorite. Low-silica diorite in the Lindeques Drift Intrusion was produced by the reaction of the parental magma with the dolomitic country rock of the Chuniespoort Group through desilicificaton and de-alumination. The Roodekraal Complex is composed of multiple flows of predominantly mugearite lava with sub-flow intrusions of diorite. The diorite of Lindeques Drift and the lava and diorite of Roodekraal are chemically comparable in terms of both major and trace elements, suggesting a co-magmatic derivation. The magma parental to the three bodies is proposed to be a low-Al ferrobasalt with alkaline affinities (MgO = 4.8%, TiO_2 =1.8%, P_2O_5 = 0.52%, $Zr/(P_2O_5 \bullet 10^4)$ = 0.02, Nb/Y=1.47, K_2O/Yb =1.3, Ta/Yb = 1.1). The latter was probably derived by deep crustal fractionation of amphibole and plagioclase from an alkali basalt(?) precursor in an embryonic continental rift setting. The probability that a gabbro dyke, stratigraphically below and perpendicular to the Lindeques Drift Intrusion, is a feeder to the latter is regarded as small.

Introduction

A number of kilometer-sized mafic igneous bodies (Figure 1) are scattered along the northern rim of the Vredefort impact structure (Boon and Albritton, 1936; Hargraves, 1961; Dietz, 1961; Martini, 1978; 1991; Albat and Mayer, 1989; French and Nielsen, 1990; Reimold and Gibson, 1996), and eastward to the town of Heidelberg, South Africa. Most prominent among these are the Roodekraal Complex (Bisschoff, 1972; Clark, 1972), the Lindeques Drift Intrusion (Nel and Jansen, 1957; Bisschoff, 1972), the Rietfontein Complex (Bisschoff, 1999), the Heidelberg Intrusion (this study), the Kaffirskraal Complex (Frick, 1975; 1979), and the Losberg Intrusion (Jansen, 1954). Current research indicates that these bodies, with the exception of the Losberg Intrusion, are members of a syn-Bushveld high-Ti igneous suite (acronym: HITIS), first recognized by De Waal and Armstrong (2000). The HITIS rocks typically contain augitic to salitic clinopyroxene, plagioclase ($An_{<50}$), magnetite (-ilmenite) and late magmatic amphibole (edenite-magnesiohastingsite) as dominant minerals (De Waal, unpublished information).

This paper deals with the geology and age of emplacement of the Lindeques Drift (LI) and Heidelberg (HI) Intrusions and the Roodekraal Complex (RC), as representatives of the HITIS in the Vredefort area. Earlier workers (Nel and Jansen, 1957; Bisschoff, 1972; Clark, 1972) gave attention to the general geology and petrography of the rocks of the LI and RC, but little is known about their geochemistry and mutual

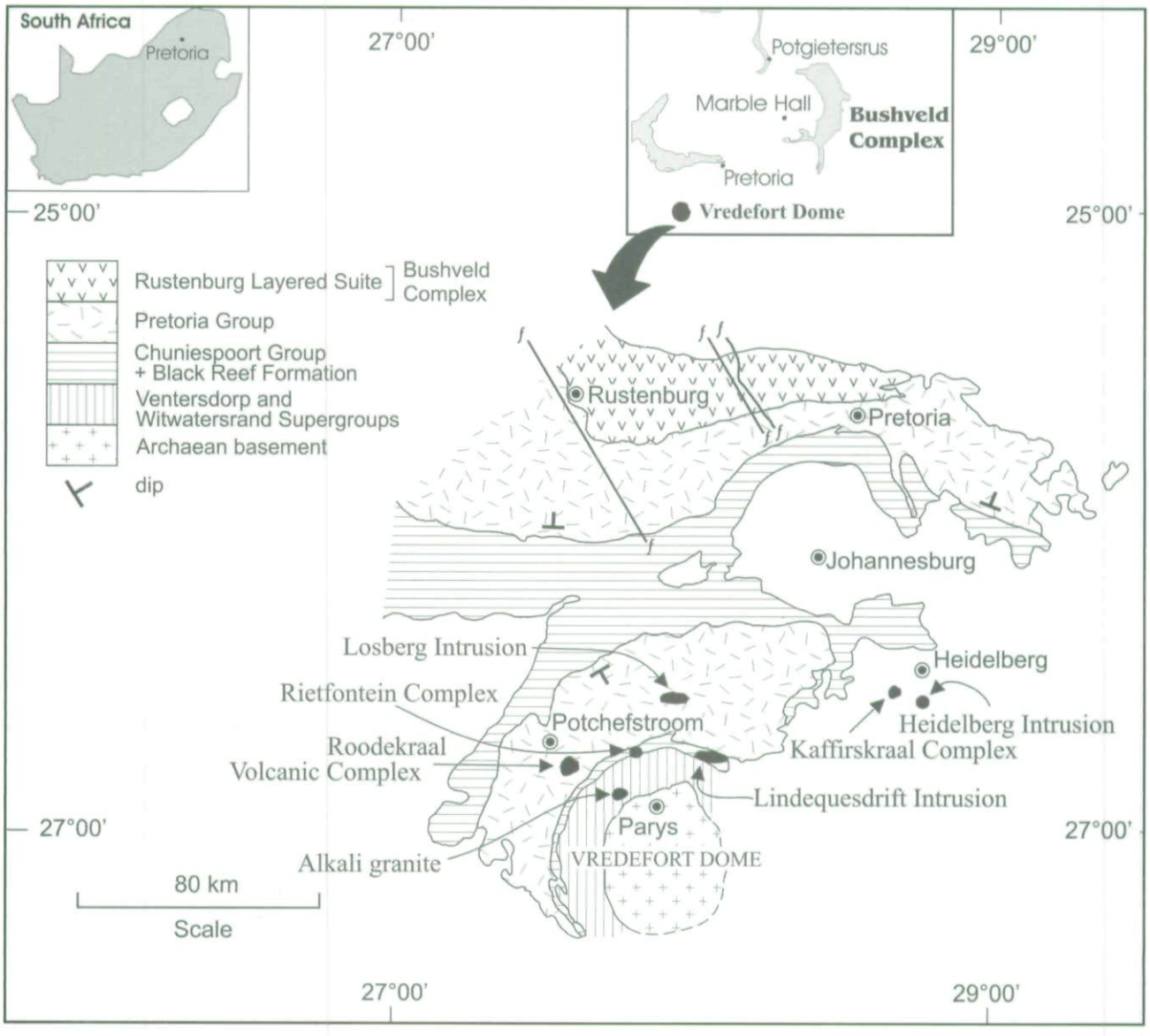

Figure 1. Geographic distribution of the HITIS rocks in the Vredefort area. The Losberg Intrusion is excluded from the HITIS group but shown here for comparison.

relationships. We expand on the existing petrographic descriptions and report zircon SHRIMP ages for the LI and RC. We also give a brief description of the HI, of which no previous record exists in the literature. We use the geochemistry to derive a genetic model for the different rock types and present arguments that the RC represents extruded residual magma of deep-seated fractionating systems genetically related to the LI and HI. The feeder status of a gabbroic dyke in the vicinity of the LI is investigated, and the significance of the HITIS in the context of the Bushveld magmatic event is briefly discussed.

Study material and methods of investigation

The rocks used in this study derive from:

1. a suite of outcrop samples from the LI, a possible feeder dyke (Bisschoff, 1999) to the LI, and the RC,
2. core sections of two boreholes drilled through the LI on Oorbietjesfontein 20 (borehole OB1) and Woodlands 192 (borehole W1) (the boreholes were drilled in a northeasterly direction at angles of 50° (OB1) and 45° (W1), respectively, to the horizontal plane), and
3. core sections of a vertical borehole (borehole P31) drilled through the HI on the farm Elandsfontein 412 ER.

The methods of investigation are summarized in Appendix 1

.

Results

Field Relations

The LI (Nel and Jansen, 1957; Bisschoff, 1972; 1999) (Figure 2) is situated approximately 50 km due west of Potchefstroom on the farms Oorbietjesfontein 20, Woodlands 192, Boschdraai 33 and Vaaldraai 277. Outcrops are poor but field observation suggests that it forms a semi-concordant sill with an estimated thickness of about 150 to 200 meters. It outcrops over a total

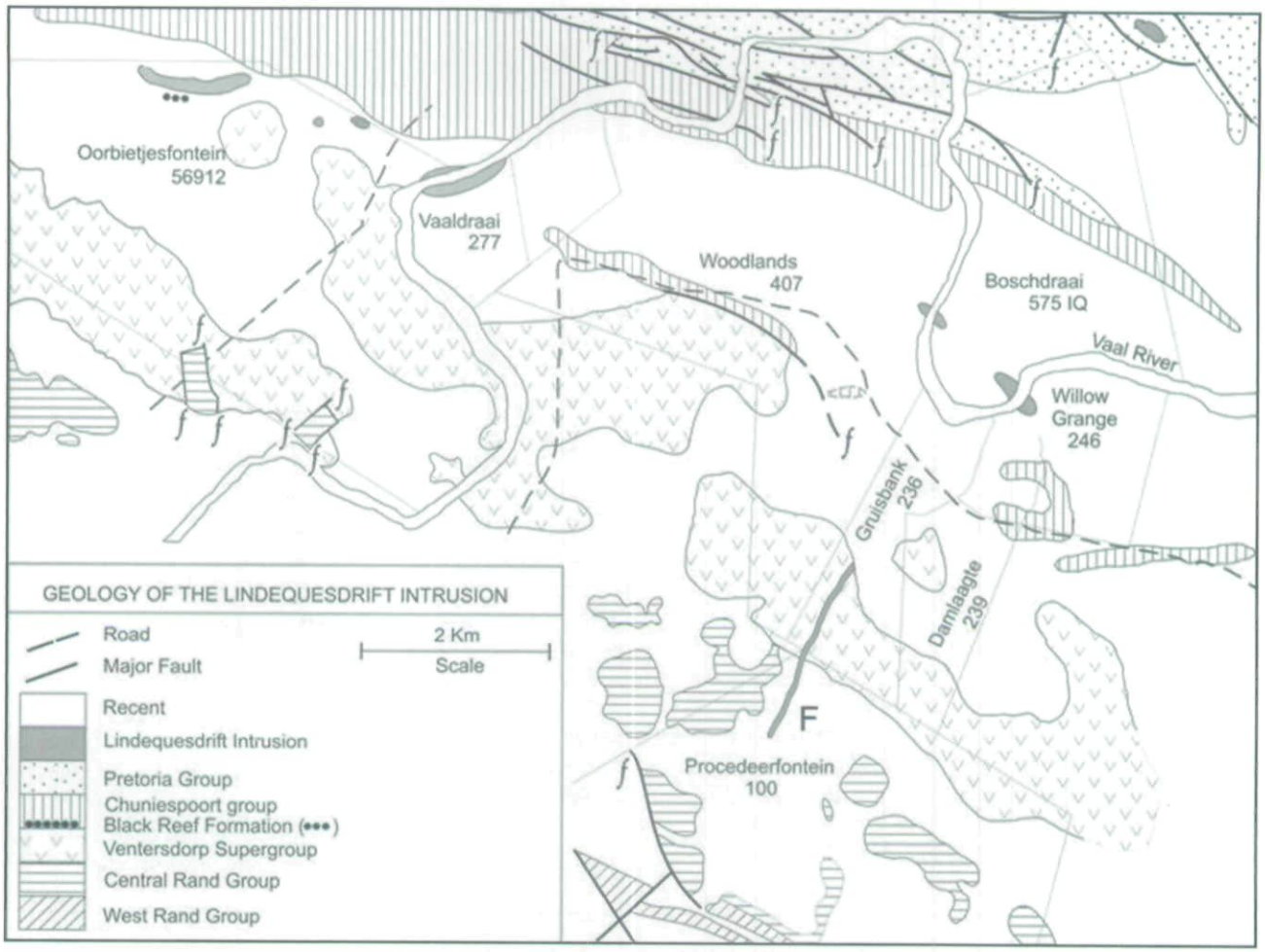

Figure 2. The Lindeques Drift Intrusion. The dyke (*f*) on the farm Gruisbank 236 and Procedeerfontein 100 was considered by Bisshoff (1999) to be a possible feeder to the intrusion. Map adapted after Bisschoff (1999).

distance of 11 km and, proceeding from west to east, the body seems to cut upward into higher levels of the dolomite(-chert) host rock succession of the Malmani Subgroup, Chuniespoort Group (age: 2549 ± 2.6 Ma; Walraven and Martini, 1995) of the Transvaal Supergroup. The LI is cut by pseudotachylite veins related to the Vredefort impact event (age: 2023 ± 4 Ma; Kamo *et al.*, 1996), a feature common to all the HITIS rocks in the Vredefort area. The impact event caused both the sill and enclosing dolomite to be overturned to the north, with dips between 60 and 70 degrees to the south.

To the south-southwest of Boschdraai, on the adjoining farms Gruisbank 236 and Procedeerfontein 100 (Figure 2), a gabbro dyke cuts though the metalava of the Ventersdorp Supergroup. This dyke has a strike perpendicular to that of the LI, and Bisschoff (1999) speculated that it could be a feeder to the latter intrusion.

The Heidelberg Intrusion is situated about 95 km south of Pretoria on the farm Elandsfontein 412 ER, Heidelberg District, where it sub-outcrops underneath a 45-meter thick cover of sedimentary rocks of the Karoo Supergroup. Because the intrusion is known only from a single borehole intersection, its shape is not known. The country rock appears to be the Turffontein Subgroup of the Central Rand Group.

The Roodekraal Complex (Bisschoff, 1972; Clark, 1972) forms a series of low hills 10 km south of Potchefstroom on the farms Roodekraal 37, Plessiskraal 43 and Prinsloosrust 93. The Complex is slightly oblong with a NS-striking long axis of about 6 km. It sits unconformably with unsheared contacts (Clark, 1972) on tilted quartzite, shale and Hekpoort lava (Rb-Sr age = 2224±21 Ma; Burger and Coertze, 1975) of the Pretoria Group. The Complex has a crude concentric morphology with an outer rim of 'andesitic' lava, a central zone of medium- to coarse-grained diorite and an intermediate zone of fine-grained diorite (Bisschoff, 1972; Clark, 1972). The diorite probably represents a series of sill intrusions below the initial lava pack. The Roodekraal rocks are cut by pseudotachylite related to the Vredefort impact event, bracketing their age to 2023 Ma<Roodekraal<2224 Ma.

Petrography

The LI is composed of spessartite, diorite, syenodiorite and feldspathic pegmatite. The spessartite has two distinct varieties. The most primitive rock is an even-grained speckled spessartite which is a medium-grained rock with euhedral clinopyroxene (± 1 mm diameter) and magnetite (-ilmenite) (< 1 mm diameter) set in a matrix of plagioclase, amphibole, magnetite, ilmenite,

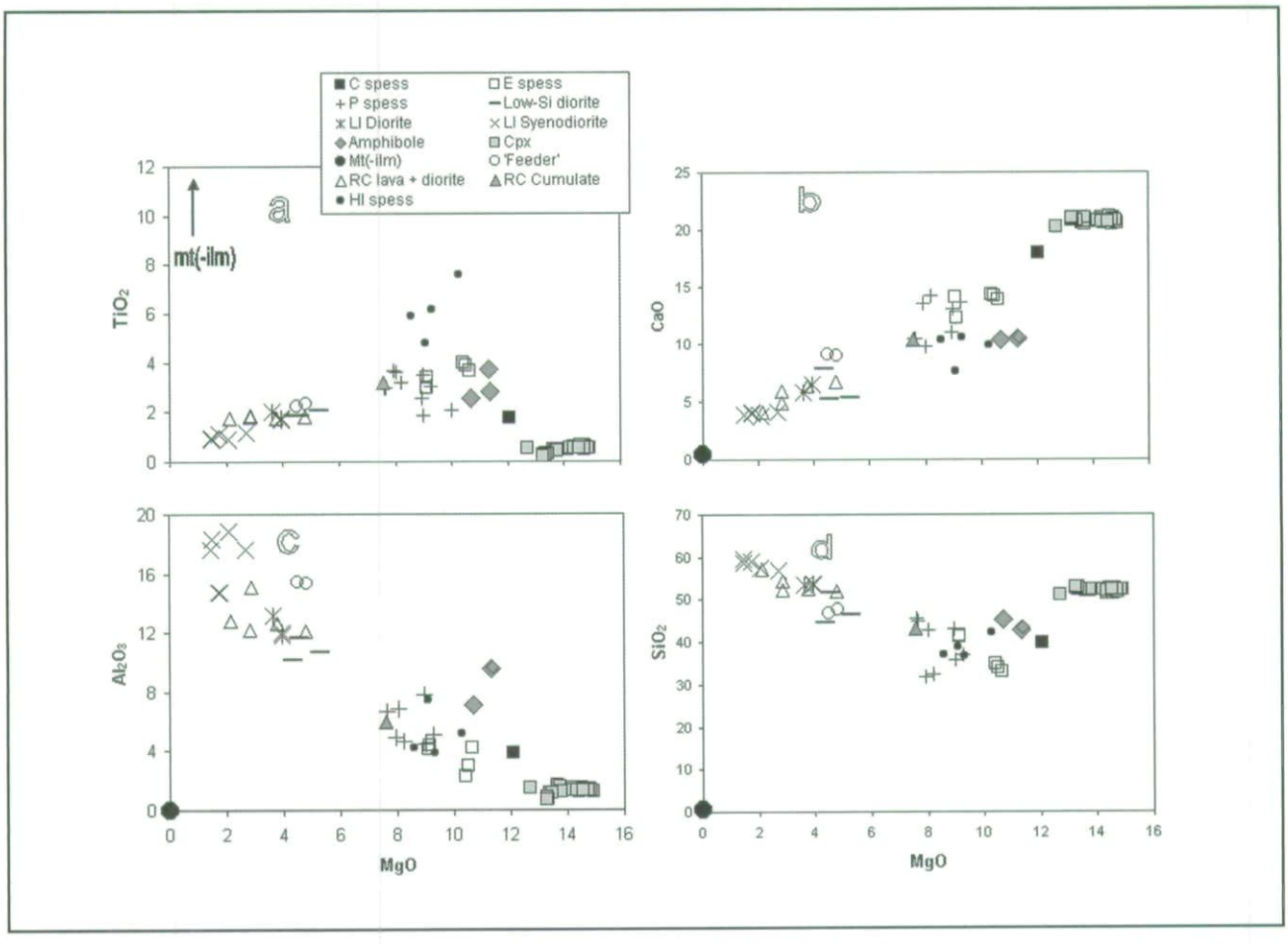

Figure 3. Major element variation diagrams of (**a**) TiO_2, (**b**) CaO, (**c**) Al_2O_3 and (**d**) SiO_2 against MgO. The spessartitic and dioritic rocks cluster in two distinct groups but overall define linear trends (LI = Lindeques Drift, RC = Roodekraal, HI = Heidelberg, C = contaminated, E-g = even-grained, P = porphyritic, spess = spessartite, Cpx = clinopyroxene, Mt = magnetite, Ilm = ilmenite). Average amphibole and a series of clinopyroxene compositions from this study are shown. Legend applies to all four sub-diagrams.

sphene, biotite, apatite and sulphide. Rarely, in some sections, relatively large prisms (up to 7 mm in length and 1.2 mm in cross sectional diameter) of anhedral clinopyroxene are scattered through the rock. Clinopyroxene (50 to 60 volume %), plagioclase (10 to 15 volume %), and magnetite(-ilmenite) (10 to 20 volume %) are the dominant minerals in the even-grained spessartite. Apatite forms small oblong needles and sphene is present in the typical sphenoidal cross sections or as irregular masses replacing ilmenite. Sulphide blebs (mm-sized) are common and dominated by chalcopyrite. Magnetite contains abundant ilmenite exsolution lamellae and segregations. Amphibole as anhedral, interstitial brownish crystals with greenish rims (5 to 10 volume %), seldom reaches dimensions much more than that of the surrounding clinopyroxene. The amphibole is randomly scattered through the rock resulting in an overall speckled, homogeneous texture. Even-grained spessartite dominates the core drilled on Woodlands (borehole W1) and is only sporadically present in the core from Oorbietjesfontein (borehole OB1).

The even-grained spessartite grades into distinctively porphyritic spessartite, which is the dominant variety on Vaaldraai (river section, Figure 2) and Oorbietjesfontein (borehole OB1). In contrast to the even-grained spessartite, this rock has less clinopyroxene (40 to 50 volume %), plagioclase is more abundant (~15 to 25%) and the late magmatic amphibole crystals have grown conspicuously large (up to 20 mm in diameter) and may reach up to 70 volume % (median ~15%) of the rock. These phenocrystic amphibole crystals, with brown cores and narrow greenish rims, tend to be euhedral but completely anhedral forms are also present. Corroded remnants of clinopyroxene and magnetite (-ilmenite) are consistently enclosed in the phenocrysts suggesting partial replacement of these minerals. Brown to green, often kink-banded, biotite is interstitial to the clinopyroxene, plagioclase and amphibole. Minor sphene, apatite, sulphide and microperthite are present.

The paragenetic sequence in the LI spessartite is magnetite(-ilmenite)-clinopyroxene-apatite-(amphibole/plagioclase)-sphene-biotite. Of these minerals clinopyroxene and magnetite (-ilmenite) are clearly cumulus phases. Plagioclase and amphibole crystallization may have overlapped to some extent. Alteration products include chlorite, epidote, saussurite, and calcite.

Dykes and sills of diorite and syenodiorite crosscut the spessartite. In the diorite, magnetite (-ilmenite) is a

Table 1. Clinopyroxene compositions

	LI Even-grained spessartite		LI Porphyritic spessartite		LI Enclosed		"Feeder" Gabbro		RC Diorite		RC Lava	
n	26		10		16		18		8		9	
	Mean	sd	Mean	sd	Mean	sd	Mean	sd	Mean	sd	Mean	sd
Raw data (EMP)												
SiO_2	52.01	0.36	51.64	0.63	50.98	1.3	51.32	0.61	50.96	0.25	51.33	0.45
TiO_2	0.54	0.07	0.55	0.08	0.58	0.12	1.06	0.17	0.96	0.14	0.84	0.2
Al_2O_3	1.38	0.11	1.56	0.22	1.64	0.42	2.55	0.44	0.98	0.26	1.09	0.34
Cr_2O_3	0.01	0.01	0.01	0.01	0.02	0.01	0.02	0.02	0.05	0.08	0.01	0.08
FeO	9.68	0.58	10.87	0.29	10.63	0.26	10.55	0.42	12.05	0.97	11.31	0.93
MnO	0.26	0.02	0.39	0.02	0.38	0.03	0.26	0.02	0.3	0.07	0.26	0.1
NiO	0.01	0.01	0.01	0.01	0.01	0.01	0.02	0.01	0.02	0.11	0.09	0.13
MgO	14.33	0.52	11.79	0.31	11.63	0.35	14.16	0.39	12.9	0.72	14.17	0.62
CaO	20.73	0.2	21.67	0.14	21.83	0.21	18.28	0.55	20.01	0.27	19.45	0.41
Na_2O	0.42	0.03	0.8	0.1	0.82	0.07	0.32	0.04	0.57	0.19	0.58	0.19
K_2O	0	0	0.01	0.01	0.01	0.01	0.02	0.02	0.02	0.02	0.02	0.04
Total	**99.37**		**99.31**		**98.54**		**98.56**		**98.79**		**99.14**	
Corrected for ferrous/ferric iron												
SiO_2	52.01		51.64		50.98		51.32		50.96		51.33	
TiO_2	0.54		0.55		0.58		1.06		0.96		0.84	
Al_2O_3	1.38		1.56		1.64		2.55		0.98		1.09	
Cr_2O_3	0.01		0.01		0.02		0.02		0.05		0.01	
Fe_2O_3	1.5		1.73		2.32		0		2.09		2.72	
FeO	8.34		9.31		8.55		10.55		10.17		8.87	
MnO	0.26		0.39		0.38		0.26		0.3		0.26	
NiO	0.01		0.01		0.01		0.02		0.02		0.09	
MgO	14.33		11.79		11.63		14.16		12.9		14.17	
CaO	20.73		21.67		21.83		18.28		20.01		19.45	
Na_2O	0.42		0.8		0.82		0.32		0.57		0.58	
K_2O	0		0.01		0.01		0.02		0.02		0.02	
Total	**99.52**		**99.48**		**98.77**		**98.56**		**99**		**99.42**	
Cations per 6[O]												
Si	1.956		1.962		1.954		1.939		1.951		1.947	
Al^{VI}	0.044		0.038		0.046		0.061		0.044		0.049	
Al^{IV}	0.016		0.032		0.028		0.052		0		0	
Fe^{3+}	0.042		0.049		0.066		0		0.06		0.077	
Cr	0		0		0		0.001		0.002		0	
Ti	0.015		0.016		0.017		0.03		0.028		0.024	
Fe^{2+}	0.261		0.295		0.272		0.334		0.324		0.28	
Mn	0.008		0.013		0.012		0.008		0.01		0.008	
Ni	0		0		0		0		0		0.003	
Mg	0.803		0.668		0.665		0.797		0.736		0.801	
Ca	0.835		0.882		0.897		0.74		0.821		0.791	
Na	0.031		0.059		0.061		0.023		0.042		0.042	
K	0		0.001		0		0.001		0.001		0.001	
Total	**4.013**		**4.015**		**4.02**		**3.987**		**4.018**		**4.024**	
Wo	42.2		44.9		45.4		38.9		41.2		39.5	
En	40.6		34		33.7		41.9		36.9		40.1	
Fs	15.7		18.1		17.8		18		19.7		18.3	
Ac	1.6		3		3.1		1.2		2.1		2.1	

sd = standard deviation. Calculations adapted from spreadsheets of Jeremy Preston available at http://www.abdn.ac.uk/geology/profiles/analysis/software.htm

Table 2. LI and HI whole rock chemistry

	LI Contam spess	LI Even-grained mean	sd	LI Porphy-ritic spess mean	sd	HI Porphy-ritic spess. mean	sd	LI Low silica diorite mean	sd	LI Diorite mean	sd	LI Syeno-diorite mean	sd
Major % (XRF)													
n	1	5		8		4		3		3		6	
SiO	39.78	36.96	4.15	39.16	5.59	38.61	2.48	47.54	3.58	53.51	0.12	58.43	1.02
TiO_2	1.76	3.57	0.39	3.18	0.38	6.11	1.15	1.92	0.14	1.82	0.15	1.03	0.12
Al_2O_3	3.89	3.61	0.91	5.91	1.25	5.2	1.63	10.84	0.73	12.36	0.72	16.99	1.81
Fe_2O_3	21.33	29.36	2.71	26.63	3.54	25.44	4.09	16.94	1.92	13.96	0.2	8.42	0.87
MnO	0.29	0.3	0.04	0.3	0.05	0.31	0.05	0.26	0.02	0.19	0.01	0.12	0.02
MgO	12.08	9.96	0.77	8.33	0.65	9.31	0.71	4.72	0.49	3.85	0.18	1.87	0.46
CaO	17.92	13.77	0.86	12	1.76	9.58	1.36	8.21	0.65	6.22	0.41	3.93	0.14
Na_2O	1.45	1.19	0.57	2.31	0.44	2.25	0.29	6.12	1.45	4.67	0.39	6.33	1
K_2O	0.3	0.31	0.15	0.6	0.27	0.57	0.13	1.16	0.36	1.16	0.06	1.29	0.41
P_2O_5	0.33	0.12	0.07	0.23	0.11	1.42	0.32	0.44	0.05	0.48	0.13	0.39	0.08
LOI	1.02	-0.24	0.4	0.38	0.42	0.83	1.03	0.48	0.27	0.77	0.62	0.89	0.31
Total	**100.15**	**98.91**		**99.02**		**99.62**		**98.64**		**99**		**99.69**	
Trace ppm (XRF)													
n		6		5		4		2		1		2	
Ni	82	101.4	31.3	66.1	17.4	159.5	15.6	31.1		15.8	–	3	–
Cu	1168	2291.4	1629.6	699.8	270.6	1131	580.6	161.7		267.4	–	34	–
Zn	114	139.4	17.3	137.3	20.8	191.8	49.2	98.3		131	–	69.8	–
Ga	14	15.4	10.3	17.9	6.3	14.5	2.1	23.2		17.3	–	15.8	–
Rb	12	10.2	3.9	17	8.3	16.7	2.9	30.2		24.4	–	40.4	–
Sr	72	103.8	42.9	340	168.5	318.5	166.4	446.5		404.4	–	562.9	–
Y	18	15	4	17.6	2	24.3	13.2	19.4		19.2	–	18.2	–
Zr	71	61.2	21.4	74.5	27.4	77.8	43.5	93		146	–	132.8	–
Nb	6	8.8	4.9	6.9	2.6	23.7	7.4	14.1		7.9	–	6.3	–
Mo	2	5.4	6	2.4	1	3.5	2.1	3.4		1	–	1	–
U	0	1.5	0	1.8	0.6	-	-	3.2		3	–	3	–
Th	0	2.2	1.6	2.2	1.4	5	-	5.2		5	–	5	–
Pb	1.5	4.6	3.2	5.9	4.3	10.3	4	5		1	–	1	–
Co	122	160	10.3	140.8	27.9	147.8	29.4	80.7		–	–		–
Cr	50	74.4	10.9	47.1	13.7	167	157.6	46.5		–	–	4	–
V	600	1027.6	133.2	801.8	214.3	643	233.7	270.4		318.2	–	69.1	–
Sc	33	39.6	3	34.7	8.7	23.3	10.7	12.2		21	–	10	–
S	1106	2077	1282.7	925.8	361.5	1097	674.2	219.8		–	–	–	–
REE ppm (ICP-MS)													
n		2		3		2		1		1		2	
La		3.8	–	11.1	0.1	33.2	–	12.8		17.2	–	18.4	–
Ce		9.3	–	24.6	0.1	67.1	–	26.9		35.9	–	39.3	–
Pr		1.4	–	3.3	0.1	7.8	–	3.5		4.4	–	4.5	–
Nd		6.9	–	14.8	0.9	31.6	–	14.9		18.2	–	18.1	–
Sm		1.8	–	3.3	0.2	5.9	–	3.2		3.8	–	3.5	–
Eu		0.6	–	1	0.1	1.9	–	1.1		1.2	–	1.4	–
Gd		2	–	3.4	0.4	5.6	–	3.4		3.5	–	3	–
Tb		0.3	–	0.5	0	0.7	–	0.5		0.6	–	0.5	–
Dy		1.9	–	3	0.2	4	–	3.1		3.3	–	2.8	–
Ho		0.4	–	0.6	0	0.8	–	0.6		0.7	–	0.6	–
Er		1	–	1.6	0.1	1.9	–	1.8		2	–	1.6	–
Tm		0.1	–	0.2	0	0.2	–	0.3		0.3	–	0.2	–
Yb		0.9	–	1.4	0	1.4	–	1.6		1.8	–	1.5	–
Lu		0.1	–	0.2	0	0.2	–	0.2		0.3	–	0.2	–

Table 3. LI, 'feeder' and RC whole rock compositions

	LI 'Feeder'		RC Lava*		RC Cumulate*	RC Diorite*	RC Lava**		RC Diorite**	
n	**2**		**4**		**1**	**1**	**18**		**4**	
Major % (XRF)										
	mean	**range**	**mean**	**stdev**			**mean**	**stdev**	**mean**	**stdev**
SiO_2	47.18	1	53.98	2.46	43.17	52.18	51.31	1.12	51.72	1.44
TiO_2	2.28	0.09	1.77	0.03	3.2	1.84	1.77	0.15	1.9	0.14
Al_2O_3	15.38	0.14	12.41	0.35	5.94	15.13	11.72	0.6	12.06	1.43
Fe_2O_3	14.21	0.55	13.01	0.63	23.32	12.24	15.23	2.05	15.79	1.66
MnO	0.21	0.01	0.19	0.02	0.37	0.17	0.18	0.05	0.19	0.04
MgO	4.66	0.31	3.37	1.15	7.57	2.85	2.89	0.62	4.16	1.21
CaO	9.06	0.14	5.5	1.24	10.35	5.93	5.1	1.92	5.72	1.12
Na_2O	2.74	0.06	5.51	0.68	2.8	5.53	4.73	0.61	5.2	0.7
K_2O	1.02	0.18	1.78	0.49	0.91	1.32	1.81	0.6	1.6	0.17
P_2O_5	0.28	0.01	0.52	0.02	0.23	0.71	0.5	0.15	0.51	0.1
LOI	1.96	0.08	0.7	0.19	0.04	1.01				
CO_2							3.95	1.53	0.44	0.23
H_2O+							1.24	0.29	1.04	0.55
H_2O-							0.19	0.09	0.2	0.03
Total	**98.99**		**98.75**			**97.9**	**98.91**	**100.63**		**100.51**
Trace ppm (XRF)										
Ni	39	4	31	14	61	22				
Cu	44	4	351	88	171	265				
Zn	126	8	100	25	112	121				
Ga	23	1	21	11	<2	23				
Rb	43	10	26	11	31	37				
Sr	406	25	543	140	290	677				
Y	23	4	15	4	<4	21				
Zr	184	0	140	53	35	96				
Nb	17	1	19	6	17	17				
Mo	1	0	4	nd	22	<1				
U	10	1	<3	nd	<3	<3				
Th	3	1	9	nd	<3	<3				
Pb	13	2	8	6	18	6				
Co	90	6	73	7	119	70				
Cr	110	20	70	40	74	<15				
V	231	8	232	30	879	165				
Sc	13	0	11	2	25	8				
S	459	64	184	78	211	98				
Ba	354	28	nd	nd	nd	nd				
REE ppm (ICP-MS, *XRF)										
La	46*		27	6.37	16.9	22.1				
Ce	62*		51.03	9.84	33.8	45.8				
Pr			5.73	0.95	3.9	5.6				
Nd			21.48	2.58	15.2	22.8				
Sm			3.75	0.27	2.9	4.3				
Eu			1.06	0.04	0.8	1.4				
Gd			3.4	0.08	2.7	3.8				
Tb			0.48	0.01	0.4	0.5				
Dy			2.9	0.08	2.3	3.2				
Ho			0.57	0.01	0.5	0.6				
Er			1.6	0.04	1.2	1.8				
Tm			0.22	0.01	0.2	0.2				
Yb			1.41	0.06	1.1	1.5				
Lu			0.21	0.01	0.2	0.2				

nd = not determined

LI = Lindequesdrif Intrusion

RC = Roodekraal Complex

* this study, ** from Clark, 1972

prominent constituent and the clinopyroxene crystals are fine-grained and partly or wholly replaced by green amphibole. The plagioclase becomes abundant (25 to 50 volume %) and develops crystal dimensions equal to or larger than that of the clinopyroxene. Phenocrystic biotite and/or amphibole (usually less than 10 percent) form poikiliths that commonly enclose corroded crystals of plagioclase. In general, magnetite (-ilmenite) and apatite precede clinopyroxene-plagioclase in the paragenetic sequence, and the amphibole replaces these early-formed minerals.

The syenodiorite contains compositionally zoned and saussuritized plagioclase (~55 volume %), primary amphibole needles (20 volume %), green chlorite after biotite (~10 volume %), quartz (~5 volume %), K-feldspar (~5 volume %) and magnetite (-ilmenite) (~1 volume %). The plagioclase is polysynthetically twinned with clear rims of almost pure albite. The paragenetic sequence is magnetite (-ilmenite)-amphibole-plagioclase-biotite-(quartz-K-feldspar). Rarely, in some syenodiorite samples, plagioclase forms a cumulus phase.

Feldspar-rich pegmatite forms irregular schlieren (cm- to meter-sized) throughout the spessartite, but is notably less common in the diorite. Bisschoff (1972) noticed that on Boschdraai the spessartite seemingly crystallized inward from the walls of the intrusion and that pegmatite schlieren in the spessartite increase in number towards the syenodiorite core, which is largely devoid of schlieren.

Calc-silicate xenoliths, typically composed of olivine marble or fine-grained magnetite-poor clinopyroxene-plagioclase rock, are present in the spessartite. The xenoliths show distorted structures suggestive of thermal softening, rotation and partial solution in the host spessartite. Isolated plagioclase segregations in the spessartite and diorite seem to have some spatial relationship to the calc-silicate xenoliths.

The 'feeder' dyke on Gruisbank is a sub-ophitic fine- to medium-grained gabbro with 60 volume % chemically zoned and polysynthetically twinned plagioclase, 25 volume % interstitial clinopyroxene, 10 volume % magnetite (-ilmenite) and minor quartz and apatite. Clinopyroxene segregations, up to 5 mm in diameter and enclosing small blades of plagioclase (< 0.3 mm), are scattered through the rock. The gabbro is variably altered and in places contains up to 30 percent brownish-green amphibole and chlorite as a replacement of the clinopyroxene. The paragenetic sequence is plagioclase-magnetite (-ilmenite)-apatite(?)-clinopyroxene-quartz.

The main rock type in the HI is a porphyritic spessartite, which is petrographically almost identical to that of the LI. The rock contains 22 to 35 volume % (median 31) clinopyroxene, 22 to 47 volume % (median 42) amphibole, 9 to 23 volume percent (median 18) magnetite (-ilmenite), and 1 to 10 volume % (median 6) plagioclase as major minerals. The amphibole phenocrysts in the HI spessartite tend to be more anhedral than those in the LI spessartite. Apatite is a prominent accessory mineral that crystallized before magnetite (-ilmenite), which in turn was followed sequentially by clinopyroxene, amphibole, plagioclase and biotite.

As described by Bisschoff (1972) and Clark (1972), the lavas of the RC are porphyritic to non-porphyritic with phenocrysts of tabular plagioclase (< An_{34}; up to 5 mm in diameter) in a clinopyroxene-plagioclase-amphibole-magnetite(-ilmenite)-biotite-apatite matrix. Both amygdaloidal and massive lava are present. Clinopyroxene-magnetite(-ilmenite) cumulates are developed near the lower contacts of some of the flows. Alteration products include sphene, chlorite, actinolite, sericite, calcite, magnetite, epidote-clinozoisite and minor quartz.

The diorite, associated with the RC (Bisschoff, 1972, Clark, 1972), consists of magmatic plagioclase (67 to 71

Table 4. CIPW Norms

	LI C spess	LI E-g spess	LI P spess	LI Low silica diorite	LI Low silica diorite	RC Cumu-late	RC primlava	HI P spess	'Feeder' gabbro	RC lava	LI diorite	LI Syeno-diorite	Pheno-crystic edenite
Qz	–	–	–	–	–			–	–	–	3.73	4.98	–
Or	–	1.89	4.2	4.57	7.44	5.37	8.62	3.38	6.2	10.73	6.95	7.69	3.13
Ab	–	1.6	12.13	27.64	41.6	21.9	40.57	19.23	23.87	47.46	40.17	54.18	20.09
An	3.23	3.6	2.39	3.08	4.59	0.96	7.08	2.46	27.46	3.98	9.54	14.31	6.46
Lc	1.4	–	–	–	–			–	–	–	–	–	–
Ne	6.7	4.63	8.13	9.98	1.37	0.96		–	–	–	–	–	0.75
Di	53.58	52.43	43.03	31.83	24.75	39.74	18.82	29.09	14.18	16.96	15.55	2.34	36.55
Hy	–	–	–	–	–		4.32	8	14.3	9.31	12.19	8.62	–
Ol	11.53	9.52	7.38	9.87	7.29	7.17	7.39	6.03	4.58	0.15	–	–	18.33
Mt	14.07	19.36	16.54	7.9	7.5	15.24	6.02	16.84	4.26	6.75	7.23	4.95	8.93
Il	3.39	6.85	5.68	4.04	3.48	6.09	3.39	11.76	4.47	3.44	3.53	1.98	4.83
Ap	0.73	0.26	0.61	1.09	0.94	0.5	1.14	3.14	0.63	1.16	1.06	0.87	–
Fe^{3+}/Fe^{2+}	0.45	0.45	0.45	0.3	0.3	0.45	0.3	0.45	0.2	0.35	0.35	0.35	0.4
An/(An+Ab)	1	0.69	0.16	0.1	0.1	0.04	0.15	0.11	0.53	0.08	0.19	0.21	0.24

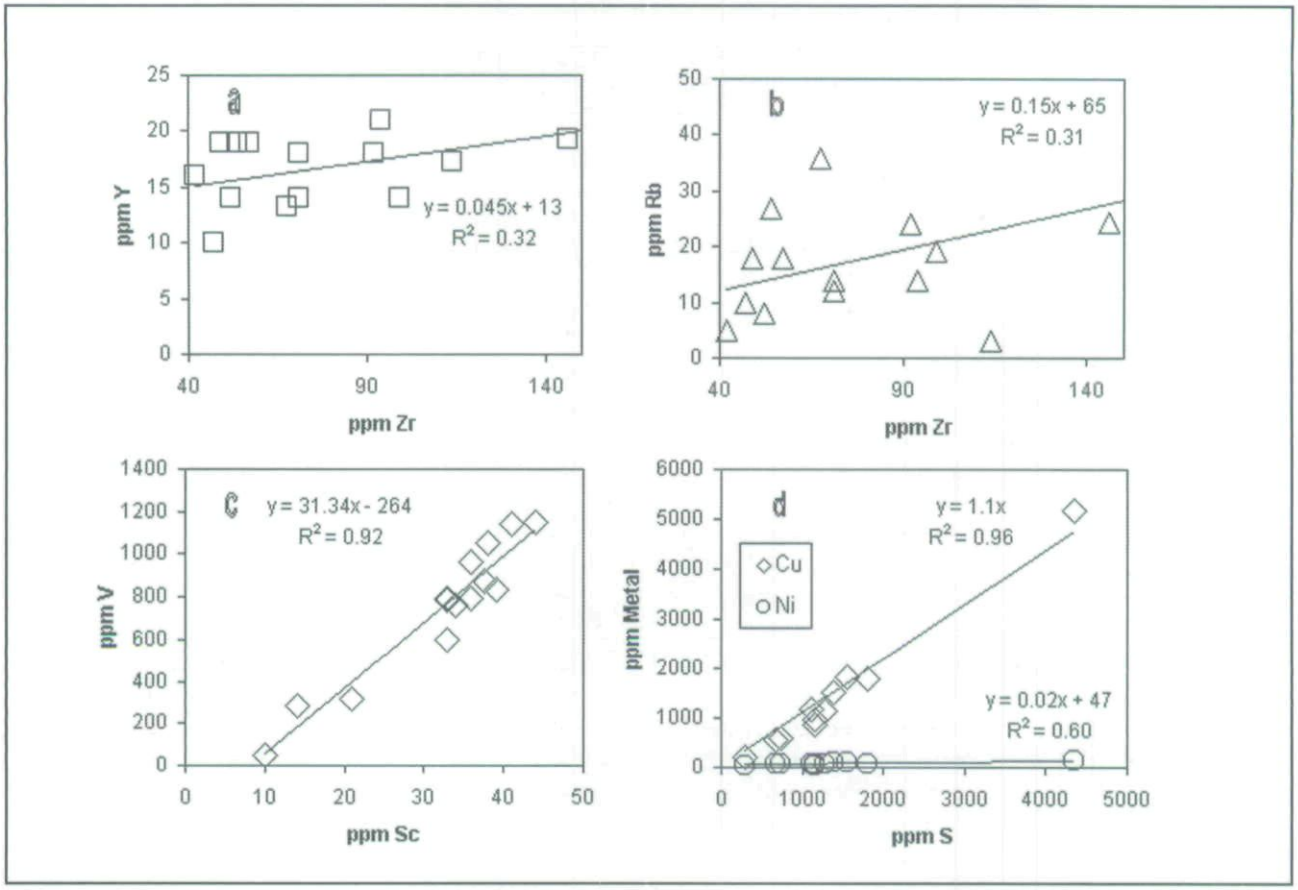

Figure 4. Trace element variation diagrams. Incompatible elements (**a** and **b**) are weakly positively correlated, whereas compatible elements (**c** and **d**) are strongly (high coefficients of variation) positively correlated. The scatter in the incompatible elements is in part due to relative mobility.

volume %; zoned, up to An_{37}), clinopyroxene (10 volume %), magnetite(-ilmenite) (7 to 19 volume %), biotite (up to 2 volume %), apatite (0.6 to 2.3 volume %), K-feldspar and olivine (rare). Late-magmatic amphibole (4 to 9 volume %) replaces clinopyroxene pseudomorphously. Secondary minerals include sphene, chlorite, stilpnomelane, sericite, calcite, magnetite, epidote-clinozoisite and minor quartz. Diorite aplite and pegmatite veins are subordinate in the RC.

Olivine is present but not a common mineral in the HITIS rocks. Clark (1972) reported a 30 m thick borehole intersection of modally layered olivine diorite, underlying a pyroxene andesite in the RC. The layer contains magnetite(-ilmenite) (up to 40 volume %, concentrated in the basal part of the layer), clinopyroxene (up to 80 volume %; concentrated in the lower and middle part of the layer), plagioclase (An_{41}; up to 45 %), orthopyroxene (En_{81}; up to 40 volume %) and olivine (Fo_{81}; up to 10 volume %). The latter three minerals are concentrated towards the top of the layer. Amphibole as a late magmatic phase replaces the pyriboles to a variable extent in these rocks.

Mineral chemistry

The clinopyroxene in the spessartite from both the LI and HI is light green in colour and forms euhedral crystals if enclosed in plagioclase, but are corroded and reduced in size when enclosed in amphibole. The most primitive clinopyroxene (Table 1), that forms the euhedral crystals in the even-grained spessartite, is an augite, $Wo_{42.1}En_{40.6}Fs_{15.7}Ac_{1.6}$ (nomenclature after Le Bas, 1962). The euhedral clinopyroxene ($Wo_{44.9}En_{34.0}Fs_{18.0}Ac_{3.0}$) in the matrix of the porphyritic spessartite and the anhedral clinopyroxene ($Wo_{45.4}En_{33.7}Fs_{17.8}Ac_{3.1}$), enclosed and partly resorbed by the amphibole phenocrysts, are both salites and statistically not chemically distinguishable. The cores of the amphibole phenocrysts are typically brown edenite to magnesiohastingsite and the greenish rims are magnesiohornblende (nomenclature after Leake *et al.*, 2004). Plagioclase in the spessartite ranges from An_{45} to $An_{<5}$ (average 12.1 ± 12.7% An; based on 16 electron microprobe analyses).

In the "feeder" gabbro, the clinopyroxene (Table 1) has an average composition of $Wo_{38.9}En_{41.9}Fs_{18.0}Ac_{1.2}$ and the plagioclase ranges between An_{69} and An_{76}. These high anorthite contents of the "feeder" dyke distinguish it from the rocks of the LI, HI and RC.

The LI diorite contains augite and magnesio-hornblende with plagioclase that ranges from An_{46} to $An_{<5}$ (average 13.3 ± 12.8% An; 30 electron microprobe analyses). The augite in the RC diorite ($Wo_{41.2}En_{37}Fs_{19.8}Ac_{2.1}$) (Table 1) shows a slight enrichment in En over Fs relative to the clinopyroxene in the LI diorite. The augite ($Wo_{39.5}En_{40.1}Fs_{18.3}Ac_{2.1}$) in the RC lava

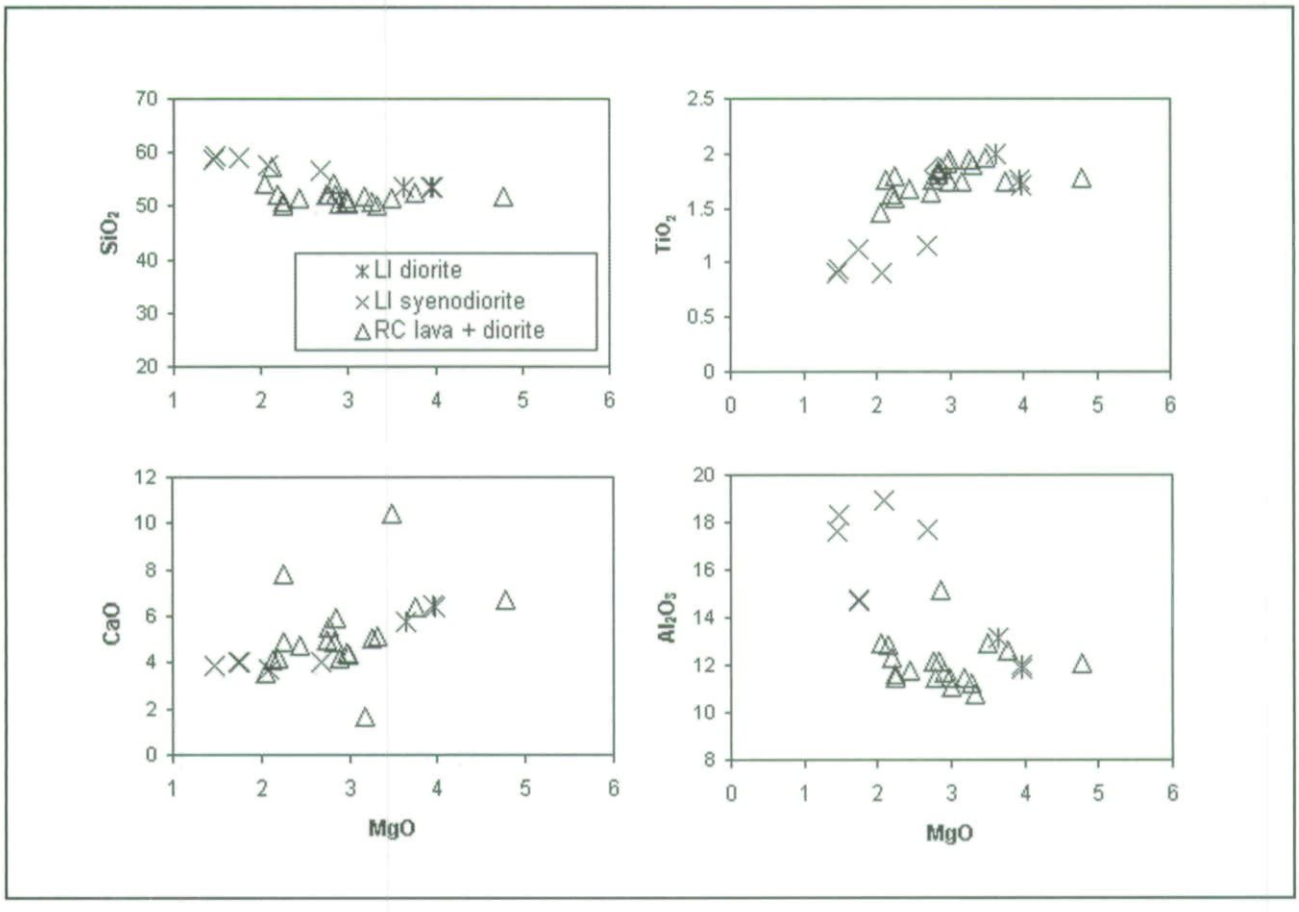

Figure 5. Major element concentrations in the LI diorite and syenodiorite compare well with those of the RC lava for comparable MgO concentrations. Legend applies to all four sub-diagrams. Data for 'RC lava and diorite' include those of Clark (1972).

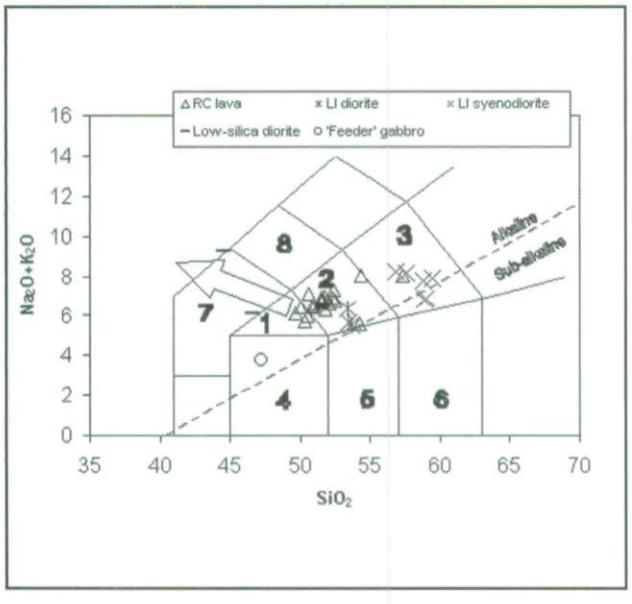

Figure 6. TAS diagram after LeBas *et al.* (1986). The data (this study and from Clark, 1972) for the LI and RC diorite and lava plot predominantly in the mugearite field, whereas those for the LI syenodiorite cluster in the benmoreite field. The 'feeder' gabbro plots in the alkali basalt field. The low-silica diorite forms a crudely-defined trend (arrow) away from the diorite-lava cluster (see text for detail). (1 = hawaiite, 2 = mugearite, 3 = benmoreite, 4 = basalt, 5 = basaltic andesite, 6 = andesite, 7 = tephrite, 8 = phonotephrite).

is depleted in Wo and enriched in En relative to that in the RC diorite. Plagioclase in the RC lava ranges from An_{30} to An_0 (average 8.8 ± 8.0% An, 30 electron microprobe analyses). The high sodium content of the RC lava is reflected in the late magmatic amphibole, which is dominantly a ferro-richterite with minor richterite and ferro-winchite.

Whole rock chemistry

The chemical compositions of the rocks of the LI are summarized in Table 2. Of special note here is the low-silica diorite (SiO_2 < 50%), which forms a crosscutting feature in the spessartite in the deeper parts (stratigraphically the upper part of the inverted sill) of borehole OB1. The two major groupings are illustrated in Figure 3, *i.e.* dioritic and spessartitic rocks, which in combination describe narrow linear trends. In these linear series, the even-grained spessartite is the most primitive (MgO-rich) rock, followed by the porphyritic spessartite, then diorite and finally the most evolved syenodiorite. The low-silica diorite plots on the high-MgO side of the LI diorite, and one sample, referred to as 'contaminated spessartite', falls off the main linear trends towards the clinopyroxene composition.

Correlation matrices calculated for the complete LI dataset (not shown here) confirm the trends shown in Figure 2, and show that the spessartitic

Table 5. Summary of SHRIMP U-Pb zircon data for diorite sample X386P from the Lindeques Drift Intrusion

Grain Spot	% ^{206}Pbc	ppm U	ppm Th	^{232}Th /^{238}U	ppm ^{206}Pb*	(1) ^{206}Pb /^{238}U Age		(1) ^{207}Pb /^{206}Pb Age		%-Dis-cordant	Total ^{238}U /^{206}Pb	±%	Total ^{207}Pb /^{206}Pb	±%	(1) ^{238}U/ ^{206}Pb*	±%	(1) ^{207}Pb* /^{206}Pb*	±%	(1) ^{207}Pb* /^{235}U	±%	(1) ^{206}Pb* /^{238}U	±%	err corr
1.1	0.08	188	93	0.51	55.7	1,909	±13	2,046.30	±8.5	7	2.9	0.81	0.12692	0.41	2.902	0.81	0.12625	0.48	5.999	0.94	0.3446	0.81	0.859
2.1	–	243	117	0.5	75.3	1,983	±16	2,056.60	±7.9	4	2.776	0.92	0.12686	0.44	2.776	0.92	0.12698	0.44	6.308	1	0.3603	0.92	0.901
3.1	0.21	149	66	0.46	41.2	1,797	±19	2,052	±11	12	3.103	1.2	0.12853	0.45	3.11	1.2	0.12668	0.62	5.616	1.3	0.3215	1.2	0.886
4.1	22.19	115	72	0.65	28.6	1,313	±27	2,058	±470	36	3.446	0.89	0.3218	0.76	4.428	2.2	0.127	27	4	27	0.2258	2.2	0.084
5.1	–	152	58	0.4	46.7	1,973	±15	2,061.50	±8.2	4	2.793	0.86	0.12691	0.47	2.792	0.86	0.12733	0.47	6.288	0.98	0.3581	0.86	0.879
6.1	0.24	231	115	0.51	64.6	1,812	±15	2,008	± 15	10	3.074	0.92	0.12567	0.63	3.081	0.93	0.1235	0.87	5.527	1.3	0.3246	0.93	0.729
7.1	5.1	94	37	0.41	27.9	1,824	±17	2,039	±100	11	2.902	0.92	0.1705	1.2	3.058	1	0.1257	5.7	5.67	5.8	0.327	1	0.179
8.1	11.82	228	114	0.52	66.7	1,693	±21	2,015	±250	16	2.936	0.77	0.2278	1.5	3.33	1.4	0.124	14	5.14	14	0.3003	1.4	0.101
9.1	0.93	373	104	0.29	80.4	1,430.20	± 9.7	1,857	± 22	23	3.988	0.75	0.12171	0.4	4.026	0.76	0.1136	1.2	3.889	1.4	0.2484	0.76	0.528
10.1	1.37	175	60	0.35	52.1	1,891	±20	2,057	± 67	8	2.894	1.2	0.1391	2	2.934	1.2	0.127	3.8	5.97	4	0.3408	1.2	0.312
11.1	15.86	195	79	0.42	66.1	1,852	±26	1,948	±350	5	2.528	0.88	0.2583	2	3.004	1.6	0.119	19	5.5	20	0.3328	1.6	0.084
12.1	0.06	265	112	0.44	82.4	1,990	±14	2,055.10	±6.6	3	2.763	0.79	0.12737	0.37	2.765	0.79	0.12688	0.37	6.328	0.87	0.3617	0.79	0.905
13.1	0.11	164	59	0.37	53.1	2,058	±16	2,064.20	±9.8	0	2.656	0.9	0.12853	0.49	2.659	0.9	0.12753	0.56	6.613	1.1	0.3761	0.9	0.851
14.1	0.03	267	147	0.57	87.9	2,091	±15	2,055.70	±7.5	-2	2.609	0.84	0.12721	0.42	2.61	0.84	0.12692	0.43	6.705	0.94	0.3831	0.84	0.891
15.1	7.74	264	113	0.44	70.4	1,624	±14	1,896	±150	14	3.219	0.79	0.18369	0.37	3.489	0.99	0.116	8.6	4.58	8.6	0.2866	0.99	0.115
16.1	0.12	329	165	0.52	107	2,070	±25	2,052.30	±8.1	-1	2.638	1.4	0.12769	0.4	2.641	1.4	0.12667	0.46	6.614	1.5	0.3787	1.4	0.952
17.1	0.23	218	68	0.32	63	1,868	±14	2,040	±13	8	2.968	0.85	0.12783	0.46	2.975	0.85	0.12582	0.71	5.831	1.1	0.3361	0.85	0.768

Errors are 1-sigma; Pb_c and Pb* indicate the common and radiogenic portions, respectively.
Error in Standard calibration was 0.41% (not included in above errors but required when comparing data from different mounts).
(1) Common Pb corrected using measured ^{204}Pb.

rocks are enriched in Mg, Fe, Ca, Ti, Ni, Cu, Co, Cr, V, Sc and S and depleted in Si, Al, Na, K, P, Sr, Rb, Y and Zr relative to the dioritic rocks. It is evident that the spessartite is enriched in elements compatible with the mafic minerals, whereas the diorite is enriched in the complementary incompatible elements. The incompatible trace elements are mutually positively correlated (Figures 4a and b), but show a relatively large amount of scatter (*i.e.* low coefficient of determination, R^2). In contrast, the compatible trace elements (Sc, V, Cr and Ni), also mutually positively correlated, display much less scatter (large R^2 values), as illustrated in Figure 4c.

Cu is strongly positively correlated with S (Figure 4d). The Cu/S ratio of ~1.1 for the LI approaches the expected Cu/S ratio of 1.06 for ideal chalcopyrite. Ni is largely independent of the S concentration (Figure 4d).

For most major elements, the HI spessartite (Table 2, Figure 3) is intermediate between the even-grained and porphyritic spessartite of the LI, but is notably enriched in titanium and depleted in calcium relative to the latter. This is largely a reflection of the higher amphibole and lower clinopyroxene concentrations in the HI spessartite relative to the LI rocks. The relatively high P_2O_5 content of the HI spessartite conforms to its high apatite content. In terms of trace elements there is little difference between the HI and the porphyritic LI spessartite (Table 2).

In terms of major elements, the RC cumulate plots in the spessartite cluster close to the LI spessartite (Figure 3). The RC lava and diorite are chemically comparable to the LI diorite (Tables 2 and 3, Figure 5). All these rocks are sodium-rich ($Na_2O>K_2O+2$), which on a TAS diagram (Figure 6) (LeBas *et al.*, 1986; Le Maitre, 2002) classify them as hawaiite and mugearite in the *hawaiite-mugearite-benmoreite* series. The LI syenodiorite classifies as benmoreite in Figure 6.

The "feeder" dyke (Table 3, Figure 3) is enriched in aluminium and depleted in iron and sodium relative to the LI diorite (Table 2) and plots in the alkali basalt field on the TAS diagram. The trace element chemistry of the 'feeder' dyke, the feldspathic spessartite, the LI diorite

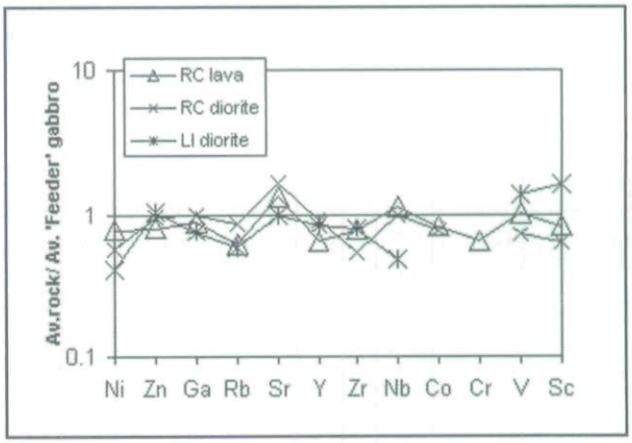

Figure 7. Spidergram comparing the trace element concentrations of the LI diorite and RC lava and diorite with the 'feeder' gabbro.

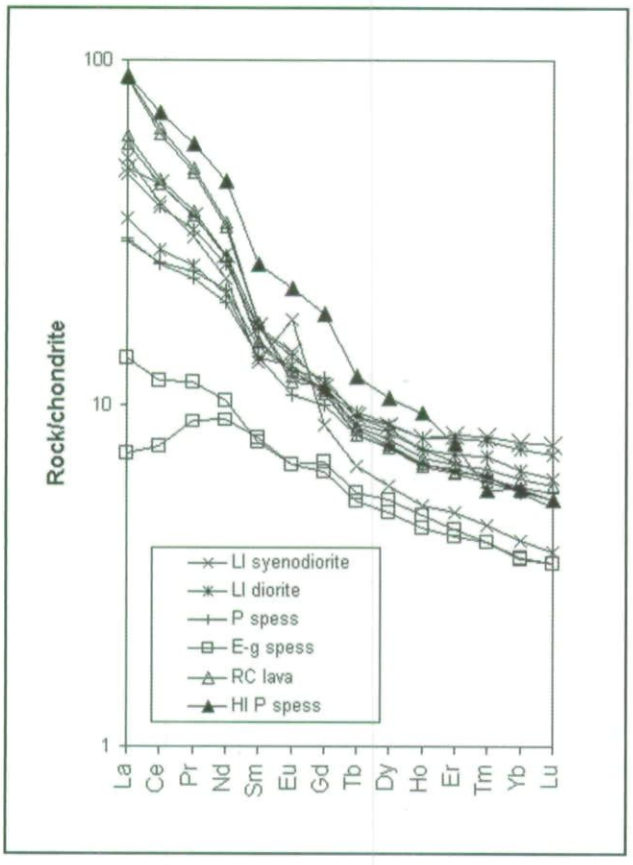

Figure 8. Chondrite-normalized REE patterns for the LI, HI and RC rocks (see text for detail).

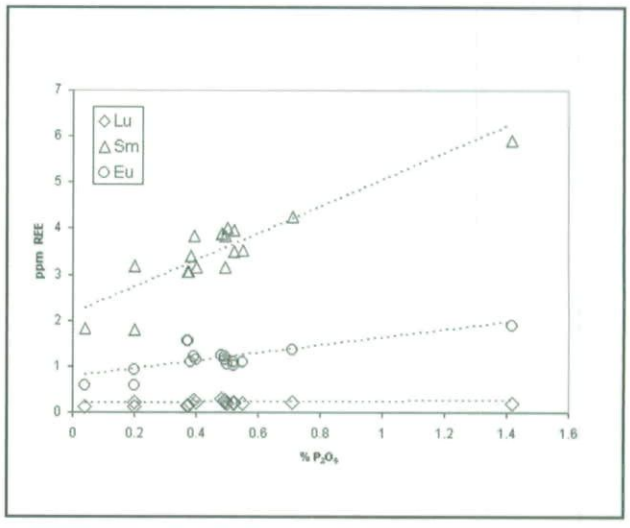

Figure 9. Concentration of selected REE in the LI, HI and RC rocks is a function of their apatite (P_2O_5) content. The lines of best fit are tentative.

and the RC rocks shows some correspondence (Figure 7), which might reflect a genetic connection.

Finally, to facilitate later discussions about possible parental magmas, we list the CIPW norms of all the major rock types in the LI, HI and RC in Table 4. Included in this list is the most primitive (MgO-rich) sample of the low-silica diorite, as well as the most primitive RC lava. It is notable that the LI, HI and RC rocks cover a wide compositional spectrum, from Ne-normative spessartite through Ol-Hy-normative intermediate rocks, to Qz-normative syenodiorite. Also, the feeder gabbro has a normative mineralogy that clearly distinguishes it from the LI-HI-RC rocks.

Rare Earth elements

The chondrite-normalized patterns (Figure 8) demonstrate a general enrichment of light over heavy REE for all the relevant rocks. The even-grained spessartite forms a distinct low-REE group, reflecting its high clinopyroxene content, whereas for the remaining LI rocks the REE concentrations gradually increase from the porphyritic spessartite, through diorite to syenodiorite. One syenodiorite sample (X385) is

Table 6. Summary of SHRIMP U-Pb zircon data for sample X743 from the Roodekraal Complex

Grain spot	% ^{206}Pbc	ppm U	ppm Th	^{232}Th /^{238}U	ppm ^{206}Pb*	(1) ^{206}Pb /^{238}U Age		(1) ^{207}Pb /^{206}Pb Age		% Dis-cordant	(1) ^{207}Pb* /^{206}Pb	±%	(1) ^{207}Pb* /^{235}U	±%	(1) ^{207}Pb* /^{238}U	±%	Err corr
1.1	0.37	126	156	1.28	37.9	1928	±14	2052	±37	6	0.12667	0.68	6.091	1.1	0.3487	0.84	0.774
2.1	0.53	92	241	2.7	24.3	1714	±13	2051	±110	16	0.1265	0.85	5.313	1.2	0.3045	0.87	0.717
3.1	3.46	101	245	2.5	27.1	1695	±22	2063	±10	18	0.1274	3.6	5.28	3.9	0.3007	1.5	0.385
4.1	0.1	116	48	0.43	37.9	2080	±15	2046	±190	-2	0.12619	0.52	6.625	0.98	0.3808	0.84	0.851
5.1	0.12	228	199	0.9	66.4	1884	±13	1872	±12	-1	0.11449	0.45	5.358	0.89	0.3394	0.77	0.863
6.1	0.08	232	95	0.42	77.2	2110	±18	2062	±22	-2	0.12734	0.37	6.798	1.1	0.3871	10	0.937
7.1	1.82	96	113	1.21	25.4	1698	±13	2022	±15	16	0.1246	1.3	5.177	1.6	0.3014	0.88	0.563
8.1	3.18	146	267	1.89	46.9	1996	±14	2034	±5.9	2	0.1253	1.5	6.27	1.7	0.363	0.82	0.492
9.1	8.88	58	87	1.56	11.6	1246	±15	1918	±19	35	0.1175	6.5	3.46	6.7	0.2133	1.4	0.204
10.1	0.05	218	60	0.29	81.2	2322	±18	2142	±15	-8	0.13329	0.4	7.97	1	0.4337	0.92	0.917
11.1	0.57	73	83	1.18	21.6	1903	±17	2034	±25	6	0.1253	0.96	5.933	1.4	0.3433	1	0.734
12.1	0.07	127	140	1.14	38	1924	±14	1877	±18	-2	0.11484	0.57	5.506	1	0.3478	0.83	0.823
13.1	2.19	129	61	0.48	24.2	1244	±20	2005	±15	38	0.1233	1.8	3.618	2.5	0.2128	1.8	0.705
14.1	0.06	137	49	0.37	49.5	2258	±25	2205	±19	-2	0.13824	0.51	7.99	1.4	0.7194	1.3	0.934

Errors are 1-sigma; Pb_c and Pb* indicate the common and radiogenic portions, respectively.
(1) Common Pb corrected using measured 204Pb

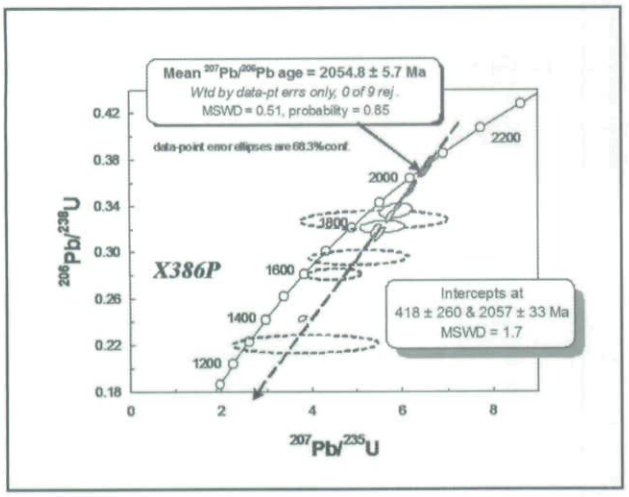

Figure 10. U-Pb concordia diagram of all SHRIMP data for zircons from diorite sample X386P. The dotted error ellipses represent those analyses with high common Pb contents. The dark grey ellipses represent the more concordant analyses used to calculate the weighted mean age of 2054±5.7Ma.

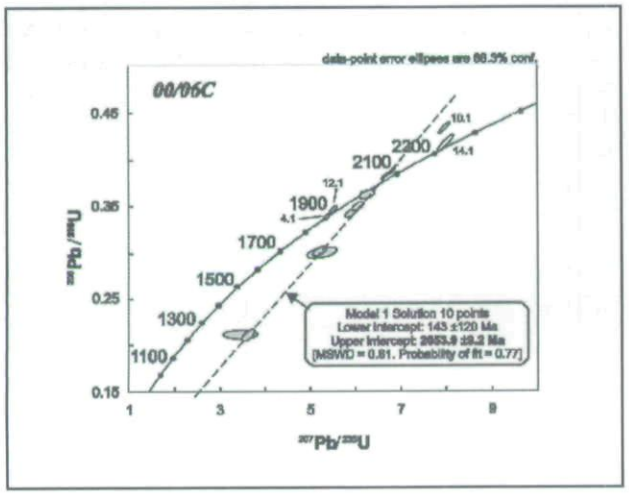

Figure 11. U-Pb concordia diagram of all SHRIMP data for zircons from diorite sample 00/06C (X743). Numbered data were discarded in calculation.

anomalous in that it displays a notably positive Eu anomaly, suggesting physical accumulation of feldspar. The lava of RC is slightly enriched in light REE and depleted in heavy REE relative to the LI diorite. The spessartite from the HI plots at high REE levels which is compatible with its high P_2O_5 content (Figure 9).

Cu mineralization

The HITIS rocks are generally enriched in Cu (Cu/Ni ratio ~ 12.5) and, as mentioned earlier, disseminated chalcopyrite is a common feature of the LI and HI rocks, especially in the spessartitic varieties. However, Cu concentrations seldom exceed 0.5 percent, which precludes economic exploitation. Clark (1972) described small Cu segregations along fault and contact zones in the RC. These hydrothermally overprinted ore bodies are zoned, ranging from magmatic high-temperature chalcopyrite-pyrrhotite-pyrite assemblages, through chalcopyrite-chalcocite, to low temperature chalcocite-bornite assemblages.

Age

Zircon grains, separated from a diorite sample (X386P) from Vaaldraai, are clear with rare inclusions, and generally anhedral (partly resorbed). Cathodo-luminescence mapping shows dominantly patchy zoning with a tendency for uranium (darker zones in CL) to increase towards the margins of the grains. Extensive alteration is present in some grains.

Seventeen grains were analyzed and the results are listed here in Table 5. Most of the analyzed spots displayed notable discordance with significant amounts of common lead present, a feature that correlates with the degree of alteration. A Concordia plot (Figure 10) for all the data yields a date of 2057±33 Ma. However, a weighted average for the grains with less than 10 percent discordance calculates to 2054.8±5.7 Ma, which is assumed to be the crystallization age of the LI.

The zircon grains concentrated from a Roodekraal diorite sample (X743; 00/06) from the farm Roodekraal 37 tended to be small (< 100 μm) and of variable form and colour suggesting a mixed population. However, the majority of the grains are subhedral, light brown and equant crystals with well-developed sector and concentric compositional zoning. These have been interpreted as "magmatic" grains formed during the crystallization of the diorite.

Fourteen analyses were done targeting mainly the "magmatic" population. The data are given in Table 6 and Figure 11. A regression of 10 analyses of "magmatic" grains yields an upper intercept age of 2053±9.2 Ma, which we interpret to be the crystallization age of the Roodekraal Complex. Four analyses are left out of the calculation. Analyses 10.1 and 14.1 (Figure 11) are probably xenocrystic zircon grains picked up by assimilation of country rock. Analyses 4.1 and 12.1 are more difficult to explain (see Discussion).

The ages reported here for the LI and RC are statistically indistinguishable from those of rocks formed elsewhere during the Bushveld magmatic event (Rustenburg Layered Suite: 2054.4 ± 2.8 Ma, R.A. Armstrong, unpublished; Lebowa Granite Suite: 2054 ± 2 Ma, Walraven and Hattingh, 1993; Rooiberg Group: 2061 ± 2 Ma, Walraven, 1997; Marble Hall diorite: 2055.6 ± 3.1 Ma, De Waal and Armstrong, 2000; Uitkomst Complex: 2044 ± 8, De Waal *et al.*, 2001).

Interpretation and discussion

'Feeder' dyke

The possibility that the 'feeder' gabbro on the farm Gruisbank (Figure 2) is a feeder to the LI needs consideration. Militating against this possibility are:

1. The 'feeder' is a gabbro with calcic plagioclase ($An_{>69}$) whereas the LI rocks typically are dioritic with sodic plagioclase ($An_{<50}$).

Table 7. Calculated cumulate mixtures (as fractions) for average spessarite

Spessartite type	Cpx	Mt	Ilm	Plag	Ol	Dol	Magma	MSD	Feasibility	Magma type	Model
Even-grained	0.5	0.22	0.03	0.05	0.02	0.04	0.14	0.01	1.72	LI Diorite	A
Even-grained	0.51	0.22	0.03	0.05	0.02	0.04	0.13	0	1.57	RC lava	B
Even-grained	0.57	0.2	0.06	0.1	0.03	0.02	0.03	0.12	10.93	'Feeder'	
Even-grained	0.23	0.17	0.02	-0.27	-0.03	0.09	0.78	0.01	5.36	Syenodiorite	
LI Porphyritic	0.33	0.17	0.02	0.06	0.04	0.04	0.34	0.01	1.97	LI Diorite	C
LI Porphyritic	0.34	0.18	0.03	0.06	0.04	0.05	0.3	0	1.59	RC lava	D
LI Porphyritic	0.49	0.16	0.04	0.21	0.08	0	0.02	0.14	16.98	'Feeder'	
LI Porphyritic	0.5	0.16	0.06	0.24	0.08	0.01	-0.05	0.05	11.24	Syenodiorite	
HI Porphyritic	0.25	0.14	0.05	0.01	0.11	0.12	0.42	0.03	1.42	LI Diorite	E
HI Porphyritic	0.36	0.15	0.06	0.04	0.12	0	0.26	0.07	5.14	RC lava	F
HI Porphyritic	0.34	0.12	0.05	-0.05	0.13	-0.01	0.41	0.23	10.09	'Feeder'	
HI Porphyritic	0.46	0.15	0.02	0.17	0.15	-0.02	0.41	0.48	28.74	Syenodiorite	

Cpx = clinopyroxene, Mt = magnetite, Ilm = ilmenite, Plag = plagioclase
Ol = Olivine MSD = Mean of the squares of the deviations. Acceptability of model increases with smaller feasibility index.

2. In the 'feeder' gabbro plagioclase is on the liquidus, whereas FeTi-oxide is the first to crystallize in the LI rocks.
3. No pseudotachylite veins have been observed in the 'feeder' gabbro. However, our sample spread (only four thin sections of this rock have been investigated) does not adequately preclude the existence of such veins.

In favour of an association of the 'feeder' gabbro with the LI rocks are:

1. The 'feeder' dyke has trace element concentration levels comparable to those of the LI-HI-RC rocks (Figure 7).
2. The disposition and orientation of the 'feeder' dyke relative to the LI suggest that the former might be a feeder to the latter.

Based on these considerations, we infer that the 'feeder' dyke might have a temporal magmatic connection with the LI, but it is not a direct feeder to the LI. This finding is supported by more detailed mass balance studies to be reported later in this paper. The possibility also exists that the 'feeder' gabbro is much younger than the LI.

Fractionation

The general linearity of the compositional data on the binary diagrams (Figure 3) and the distribution of the major and trace elements between the two main rock groups are evidently the result of crystal fractionation and accumulation. The data series formed by the diorite and syenodiorite, as well as the RC mugearite, are seen to represent the liquid trend (liquid line of descent), whereas the various spessartite rocks are the related cumulate fractions. This interpretation is fully supported by the chemical data on the RC mugearite and associated clinopyroxene-FeTi-oxide cumulate rocks.

Perusal of Figure 3 shows that simple clinopyroxene-FeTi-oxide fractionation (mass ratio ~ 75/25) can adequately explain the slopes defined by the liquid series in the different binary diagrams. To test this possibility in more detail, we employed mass balance calculations using least squares optimization (see Appendix for detail). We inferred from the paragenetic sequence that just prior to amphibole saturation the spessartite consisted essentially of clinopyroxene, FeTi-oxide and interstitial magma as well as possibly minor olivine and plagioclase. Olivine is present in the cumulate rocks of the RC (Clarke, 1972) and may have been present in the spessartite but consumed during amphibole crystallization. Minor plagioclase may have stabilized just before the onset of amphibole crystallization. We also allowed for dolomite to accommodate small amounts of carbonate assimilation, which may now be represented in the rocks as calcite and secondary chlorite (?).

We modeled average even-grained, and LI porphyritic and HI porphyritic spessartite using, sequentially, the average compositions of LI diorite, RC lava, 'feeder' gabbro and syenodiorite as possible interstitial magma components. The results, in Table 7, indicate that the LI diorite and chemically comparable LC lava consistently give the better feasibility indices (see Appendix for definition). On the strength of these models, the following inferences for the pre-amphibole mineral-magma system can be made:

1. The RC lava appears to be the most likely candidate for the interstitial magmatic component in the LI and HI spessartite. Models B, D and F (Table 7) are mutually consistent, as well as in general agreement with the mineralogical data reported earlier.
2. The LI porphyritic spessartite contained less clinopyroxene and FeTi-oxide and more trapped intercumulus magma than the even-grained spessartite when amphibole stabilized (model D vs. B, Table 7).

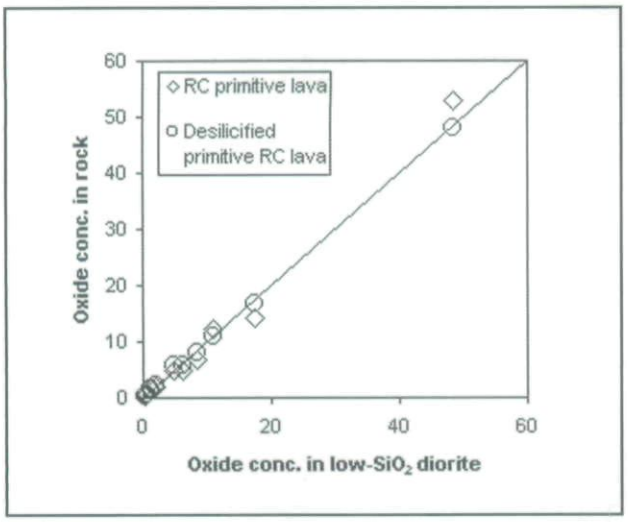

Figure 12. Simple desilicification and de-alumination (ratio SiO_2/Al_2O_3 ~ 3.6) of RC lava yields composition close to that of the low-silica diorite.

3. The final spessartite composition is a function of the weight ratio of early cumulus minerals to the amount of trapped intercumulus magma. The larger the interstitial magma content, the more felsic minerals form and higher the incompatible trace element concentrations, and *vice versa*. Consequently, the relatively small amount of trapped magma (~15%, model B) in the even-grained spessartite yielded only a few interstitial amphibole crystals (~ 7 modal % on average) which caused its speckled appearance. The more copious amounts of interstitial magma (~30%, model D), trapped in the intercumulus space of the porphyritic spessartite, accommodated more dissolved fluid and consequently crystallized more amphibole (~ 15 modal % on average). This general pattern is also reflected in the REE concentration of these rocks (Figure 8) in that the even-grained spessartite, due to its high cumulus clinopyroxene concentration, not only show marked overall depletion in REE, but also distinctly tail-off on the LREE side, relative to the porphyritic spessartite.
4. Minor plagioclase may have crystallized before the amphibole in the LI rocks, as indeed suggested by the paragenetic sequence.
5. Olivine might have been present but was consumed during amphibole crystallization.
6. The model for the HI porphyritic spessartite (model F) shows a slightly elevated feasibility index, which is largely due to an underestimation of Na_2O and Al_2O_3 in the rock. In all other respects the model is comparable to that for the LI porphyritic spessartite, except that it had more cumulus olivine. The high apatite content of the HI spessartite also suggests that the latter mineral might have accumulated together with clinopyroxene and magnetie(-ilmenite) as a cumulus mineral. Small variations in parental magma composition may well explain these observed differences.

Amphibole phenocrysts

The almost identical compositions of the partly resolved clinopyroxene remnants (LI Enclosed, Table 1) contained in the amphibole phenocrysts and the euhedral clinopyroxene in the groundmass (LI Porphyritic spessartite, Table 1) indicate that the onset of amphibole crystallization did not significantly upset the chemical equilibrium between the existing and newly precipitating phases. This observation supports the idea that the amphibole is indeed a late-magmatic phase and not the result of a metamorphic overprint.

Contamination

The presence of olivine marble and calc-silicate xenoliths in the borehole core sections of the LI suggests that chemical interaction between the siliceous dolomite country rock and the original magma is most likely. The interaction between mafic magma and carbonate rock (limestone) has been much debated (see Wyllie, 1974 and McBirney, 1984, for general discussion). The consensus is that although limestone assimilation is not important for large-scale generation of alkaline rocks, it may locally influence magma compositions. In this context, Joesten (1975) reported the reaction between a gabbroic magma and limestone in the Christmas Mountains, Texas, and showed that the magma gained Ca from and lost Si and Al to the skarned limestone, forming local segregations of pyroxenite and nepheline syenite magma in the gabbro magma, as well as a nepheline pyroxenite on the gabbro-limestone contact.

In the present study two possible processes are considered:

Desilicification and concomitant de-alumination of the initial magma due to reaction with dolomite to produce calc-silicate (mainly olivine, clinopyroxene and plagioclase) minerals.

Thermal softening and disintegration of calc-silicate aggregates under dynamic flow conditions at high temperatures, causing the newly-formed calc-silicate minerals in chemical equilibrium with the magma to physically mix with the early cumulate minerals.

The first process, as also found by Joesten (1975), may lead to locally developed nepheline normative, silica-undersaturated magma. In this study we observed that the LI spessartite and low-silica diorite in places become conspicuously feldspathic close to calc-silicate xenoliths, pointing to some reaction relationship. In addition, it can be shown that by removing 7.9 percent SiO_2 and 2.2 percent Al_2O_3 from the composition of an MgO-rich RC lava, the residual oxide concentrations closely approach those of the LI low-silica diorite (Figure 12). This suggests that the Ne-normative low-silica diorite in the LI is simply a product of desilicification and de-alumination due to interaction of the Chuniespoort dolomite with magma compositionally comparable to MgO-rich RC lava.

The second process, in keeping with Bowen's reaction rule and as was also observed by Joesten (1975), may lead to the enrichment of the cumulate

Table 8. Proposed composition of HI-LI-RC parental magma*

Major % (XRF)			
SiO_2	51.82	Cu	355
TiO_2	1.78	Rb	30.2
Al_2O_3	12.07	Sr	603
Fe_2O_3	13.82	Y	14.2
MnO	0.19	Zr	96.8
MgO	4.78	Nb	16.8
CaO	6.69	Cs	0.81
Na_2O	4.8	Ba	348
K_2O	1.46	Li	48.4
P_2O_5	0.52	La	20.9
S	0.03	Ce	41.9
LOI	0.87	Pr	4.85
Trace ppm (ICP-MS)		Nd	19.1
Hf	2.49	Sm	3.51
Ta	1.29	Eu	1.09
Pb	5.91	Gd	3.3
Th	2.77	Tb	0.47
U	0.3	Dy	2.85
Sc	16.8	Ho	0.56
V	269	Er	1.56
Cr	137	Tm	0.21
Co	55.7	Yb	1.38
Ni	50.9	Lu	0.2

*Composition of the most primitive RC lava (X876) observed in this study

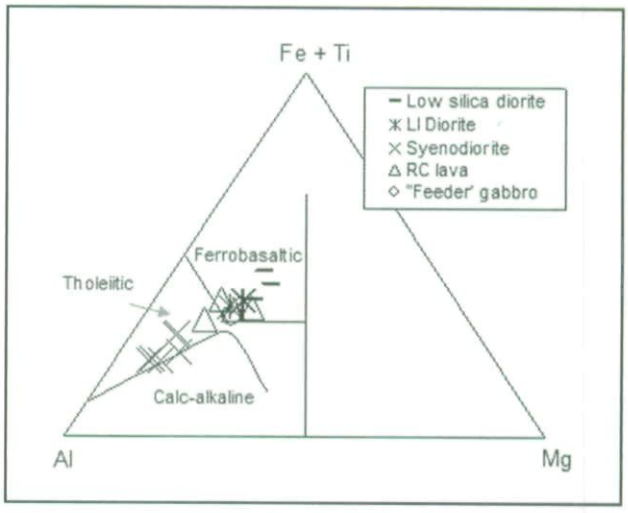

Figure 13. Jensen cation diagram (after Rollinson, 1993, and references therein) illustrating the Fe-Ti enrichment in the LI and RC diorite, lava and syenodiorite. The more primitive RC lava plots in the ferrobasalt field and the low-silica diorite plots to the right away from the Al corner, as would be expected from the proposed de-alumination process.

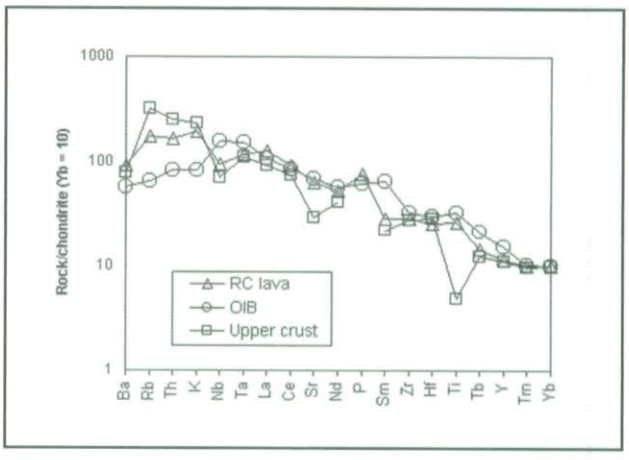

Figure 14. Chondrite-normalized spidergram (all patterns recalculated to Yb_N = 10) of the proposed parental magma compared with the upper continental crust and oceanic island basalt. The proposed parental magma mimics the upper crustal values for Ba through to Ta, but follows the OIB curve for La through to Yb. Chondrite normalization data after Thompson (1982); bulk crust after Taylor and McLennan (1985).

fraction in clinopyroxene in equilibrium with the magma. If the degree of contamination is low and the system is well mixed, its effects on whole rock chemistry will be difficult to detect. However, poor mixing of the contaminant should support local significant deviations of the cumulate mineralogy towards high clinopyroxene/plagioclase concentrations. One sample, referred to as contaminated spessartite in Table 2 and plotted in Figure 3, shows such deviation. Microscopic observation indicates that this rock has more clinopyroxene than the average even-grained spessartite, yet it is depleted in Ni, Sc and Cr (Table 2) relative to the latter, which support the notion of contamination rather than simple clinopyroxene accumulation.

Fluids and incompatible elements

The poor correlation (Figure 4) existing between the incompatible relative to the compatible trace elements is notable. All indications are that the parental magma contained small quantities of water and other volatiles. It is conceivable that as crystallization proceeded the interstitial magma became gradually enriched in these volatiles, which led to amphibole precipitation, pegmatite formation and finally an exsolved fluid phase. We envisage that channel flow regimes may have developed in the fluid-enriched interstitial magma of the compacting cumulate, which could have contributed to redistributive decoupling of the compatible and incompatible trace elements. It is to be expected that the more mobile incompatible elements, such as Rb, would show more scatter than the less immobile incompatibles such as Zr and Y (Figure 4).

In the context of possible fluid circulation, it is also necessary to look at the "younger" zircons reported in Figure 11 (samples 4.1 and 12.1, ~1.88 Ga). Zircons younger than the formation age of the host rock are not expected. Two possibilities could be considered as an explanation, *i.e.* these "younger" zircons represent laboratory contamination during mineral separation or they are the result of complex Pb-loss linked to fluid circulation and/or metamorphism. With regard to the former, it should be noted that utmost care was taken in the prior cleaning of the apparatus and that rocks younger than "Bushveld age" were not treated in the

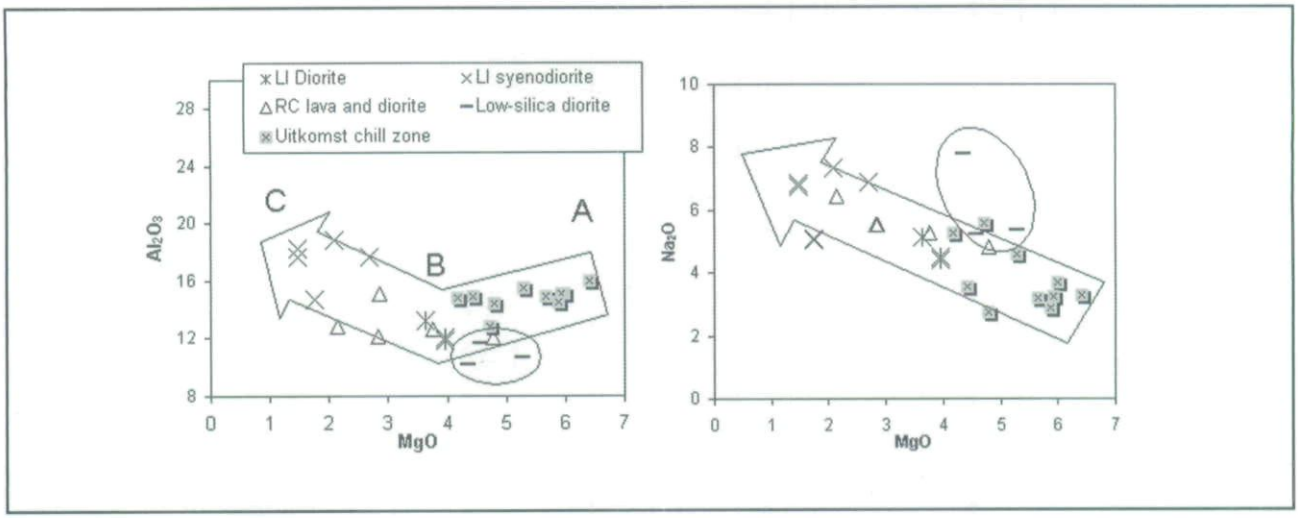

Figure 15. The Uitkomst chill zone rocks (**A-B**) define deep crustal fractionation of an alkali basaltic precursor yielding the LI-HI-RC parental magma. The latter fractionated at shallow crustal levels to produce the observed liquid series (**B-C**). For Al_2O_3 the two processes had different effects on the chemical evolution of the residual magma (hence the knick point at B), whereas for Na_2O the two processes are indistinguishable. The low-silica diorite that formed by desilicification and de-alumination of the ferrobasaltic parent is encircled (see text for detail).

relevant batch of zircon separations. We do consider laboratory contamination as unlikely.

The alternative of complex Pb-loss seems more probable. "Younger" zircons have recently been reported in SHRIMP studies on different rock types from the western Kaapvaal craton by Armstrong *et al.* (1991), Schmitz and Bowring (2000), Poujol *et al.* (2002) and Poujol *et al.* (2005). Poujol *et al.* (2005) present arguments that some of these "younger" zircons (~1.1 Ga) may reflect resorption and reprecipitation during the Namaqua orogeny. However, some "younger" zircons remain unexplained because no obvious thermal geological event seems to coincide with the measured ages. Of interest here are the two "enigmatic" reversely concordant zircons with measured ages of 1.88 and 1.78 Ga in BIF of the Amalia greenstone belt described by Poujol *et al.* (2005), which are comparable to those (1.88 and 1.87 Ga) reported in this study. There is clearly some pattern emerging, the explanation of which is beyond the scope of this investigation.

Nature and source of parental magma

If the parental magma to the LI, HI and RC is indeed represented by the MgO-rich RC lava (Table 8) as suggested earlier, the chemical characteristics of this rock could be employed to answer several important questions:

1. Was the parental magma a primary mantle melt?
2. What was the geodynamic setting of the LI, HI and RC?
3. Was the parental magma contaminated by crustal material?
4. Did the parental melt have any alkaline affinities?

In answer to the first question, the low MgO content (< 5 %) of the RC lava clearly precludes a primary mantle origin. On a Jensen diagram (Figure 13), the more primitive varieties of RC lava plot convincingly in the ferrobasalt field, attesting to their high Fe contents. Furthermore, the RC lava (Na_2O+K_2O > 6 %, Mg# = 0.25 to 0.41, Ni = 10 to 51 ppm, Cr = 4 – 137 ppm) compares well with typical ferrobasalts (enriched in alkalis, Mg# < 0.45, Ni = 50 to 100 ppm, Cr <100 pp) (BVSP, 1981). This general equivalency leads us to infer that the RC lava is a fractionated residual liquid derived from a more mafic precursor magma.

With regard to the second question, it is noted that ferrobasalt is commonly interpreted as the product of extreme olivine-plagioclase-clinopyroxene fractionation of mid-ocean ridge basalt (MORB), and typically shows flat chondrite-normalized REE patterns (Hess, 1989). However, LREE-enriched ferrobasalts have been documented, amongst other, in association with Archaean komatiites from the Munro Township, Canada (Arth *et al.*, 1977), in the Proterozoic Hartley Basalt Formation in the Northern Cape, South Africa, (Cornell *et al.*, 1998), and from volcanic ash layers in the Palaeogene Danish Basin (associated with alkaline rocks; Larsen *et al.*, 2003). Cornell *et al.* (1998) suggest an early continental rift setting for the Hartley basalt, related to the initial breakup of the Kaapvaal Craton prior to the Kheis orogenesis. Larsen *et al.* (2003) tie the ferrobasaltic ash layers in the Danish Basin to embryonic stages of rifting of proto-Iceland during the initial opening of the mid-Atlantic ridge. These observations suggest that LREE-enriched patterns in ferrobasaltic rocks are more common in early or incipient rifting (deeper, low-fraction melting), whereas flat patterns represent evolved ridge systems (shallower, high-fraction melting). Consequently, we infer that the LI-HI-RC rocks were emplaced during an incipient continental rifting episode.

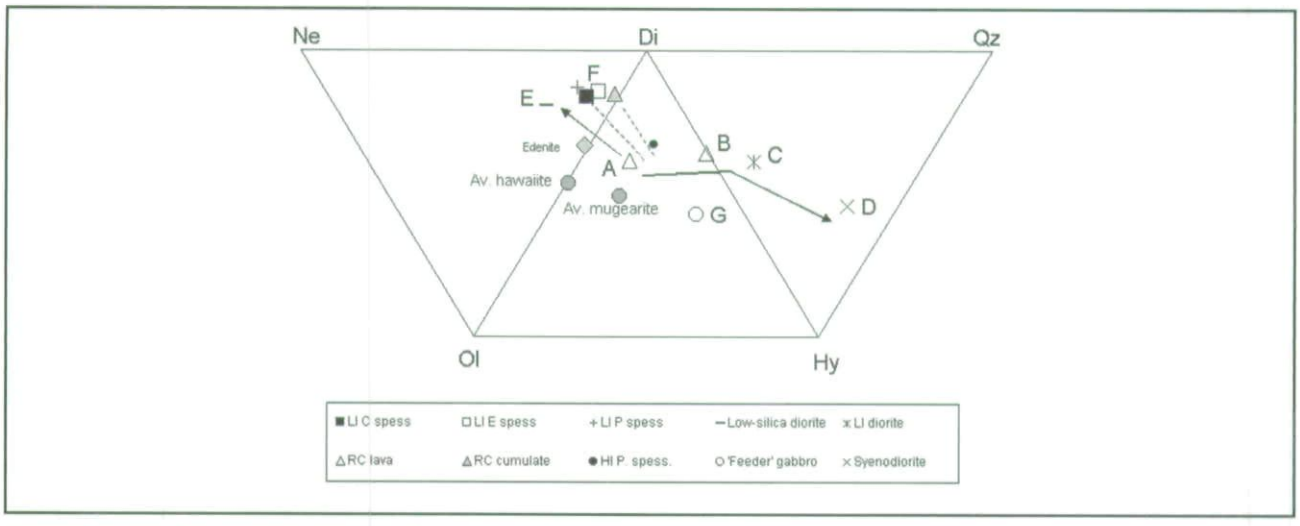

Figure 16. Ne-Ol-Di-Hy-Qz diagram illustrating the different processes that were operative in the LI-HI-RC rocks. Shallow level crustal fractionation of clinopyroxene + magnetite(ilmenite) ± amphibole±olivine defined the line of liquid descent, from a magma with composition at (**A**) (most primitive RC lava observed in this study) through (**B**) (average RC lava) and (**C**) (average LI diorite) to (**D**) (average syenodiorite). The LI and HI spessartite and RC cumulate derived from magmas with compositions somewhere between A and B (stippled tie lines). Low-silica diorite (Ne-normative) at (**E**) is a product of desilicification and de-alumination of a magma with compositions at A. Average hawaiite and mugearite after Le Maitre (1976).

To answer the third question, we investigate the trace element concentrations in the RC lava. Jakobsson (1979) illustrated that alkali basalt eruptions in post-glaciation volcanism on Iceland are connected to incipient rifting in thicker crustal sections further removed from the active mid-Atlantic ridge, where typical tholeiitic MORB is extruded. This ties in with the general pattern of lateral compositional variation of extruded basalt across the axial depression of rift zones: tholeiitic basalt being typical of the axial volcanics, yielding to alkali basalt away from the central axial line (BVSP, 1981) In addition, enriched trace element signatures in mafic volcanics in continental settings are not uncommon along continental rift zones, *e.g.* the mafic volcanics in the Tombel graben associated with the continental leg of the Cameroon line (Nkouathio *et al.*, 2002; Halliday *et al.*, 1988). In Figure 14 (a chondrite-normalized spidergram after Rollinson, 1993, and references therein), the sequence of elements from left to right are in the order of increasing compatibility in a low-fraction mantle melt, and all ratios were recalculated to Yb_N = 10 to negate effects of fractionation (Thompson *et al.*, 1983). It is evident that for the first six elements, Ba to Ta, the RC lava closely mimics upper crustal values, but for the remaining elements (to the right of Ta, excepting Sm) the RC lava seems to follow closely, absolutely and relatively, the typical oceanic island basalts pattern. These similarities cannot be fortuitous and we interpret the data to suggest that :

1. the RC lava was derived from a magma that originated in the mantle, and
2. some crustal contamination (mainly mobile large-ion lithophiles, probably by partial melt extraction) had taken place during its ascent into the crust.

In addition, the LI-HI-RC rocks are conspicuously enriched in sodium (Tables 2 and 3) and we have demonstrated that, on the TAS diagram, the RC lava plots predominantly in the mugearite field. Also, the low $Zr/(P_2O_5 \bullet 10^4)$ (0.02) and high Nb/Y (1.47) ratios as well as high TiO_2 (1.8 %) and P_2O_5 (0.52 %) contents places the RC lava well within the alkaline field (Floyd and Winchester, 1975), and the K_2O/Yb =1.3 and Ta/Yb = 1.1 ratios (Pearce, 1982) suggest that the RC lava is transitional between sub-alkalic and alkalic. Taken together, all these characteristics lead us to propose that the RC lava was derived from an alkalic mafic precursor, most probably alkali olivine basalt.

Finally, the low Al_2O_3 content (~13 % volatile free) of the predominantly mugearitic RC lava, proposed to be parental to the LI-HI-RC rocks, needs some consideration. The worldwide average for the Al_2O_3 content for mugearite, from a compilation of Le Maitre (1976), is 16.98 ± 2.11 percent (volatile free), which place the RC lava within two standard deviations from the mean, but on the low side. The explanation for the low aluminium content of the RC lava is probably to be found in amphibole-plagioclase fractionation. It is known that in 'wet' basalt melting experiments, Green (1982) found that below 10 kbar on a PT diagram the stability field boundary of amphibole has a positive slope, with clinopyroxene on the low-pressure side. This means that wet basaltic magmas can fractionate amphibole ± clinopyroxene ± plagioclase at deeper levels, but clinopyroxene ± plagioclase ± olivine are stable phases at lower pressure. De Waal *et al.* (2004) used these phase relationships to argue that the chemical variation in the chill zone of the Basal Gabbro Unit of the 2044±8 Ma Uitkomst Complex (De Waal *et al.*, 2001; De Waal and Armstrong, 2000), also a member of the HITIS, is the direct result of deep-level

Table 9. Proposed model for the formation and emplacement of the LI-HI-RC rocks

Level	Body	Process
Surface	RC	*Extrusion:* ferrobasaltic magma extrudes as mugearite lava flows and intrudes as sub-flow diorite sills
Shallow crust: Chuniespoort Group	LI	*Fractionation:* ferrobasaltic magma yields spessartite as well as dioritic and syenodioritic magma *Contamination:* ferrobasaltic magma reacts with dolomite yielding desilicified and de-aluminated low silica diorite and calcsilicate xenoliths *Late intrusion:* parental magma and differentiates (diorite and syenodiorite) from deeper intrusions form cross-cutting bodies
Shallow crust: Kimberley-Elsburg Group	HI	*Fractionation:* ferrobasaltic magma fractionates clinopyroxene, magnetite(-ilmenite), amphibole and olivine, yielding porphyritic spessartite as well as residual diorite and syenodiorite magma
Deeper crust	Staging chamber	*Fractionation:* amphibole-plagioclase fractionation of alkali basaltic magma produces ferrobasaltic (mugearitic) HI-LI-RC parental magma *Contamination:* LILE enrichment of parental magma by partial melt extraction
Mantle		*Partial melting:* deep-seated mantle melting in an incipient continental rift setting produces alkali basaltic magma

amphibole-plagioclase fractionation (weight ratio = 80/20) of a 'wet' alkaline or transitional basalt. Of interest here is that the compositions of the most evolved rocks, produced by this amphibole-plagioclase fractionation process at Uitkomst, closely approach those of the most primitive RC lavas (Figure 15). Consequently, it seems logical to infer that the RC parent is the product of deep level crustal fractionation of amphibole and small amounts of plagioclase from an alkali basaltic precursor, the latter being co-genetic with the precursor magma of the Uitkomst chill zone rocks. Since the partition coefficient, $D_{(Eu;\ amphibole/magma)}$, as a rule is smaller than both $D_{(Sm;\ amphibole/magma)}$ and $D_{(Gd;\ amphibole/magma)}$ and the reverse is true for plagioclase (Rollinson, 1993, and references therein), concomitant fractionation of these minerals will tend to cancel out and minimize the Eu anomaly. Hence the general lack of a Eu anomaly in the REE patterns of the relevant rocks.

Regional implications

Considering all the information given in the previous sections, it appears that the LI, HI and RC formed during a single magmatic event that was co-eval with the emplacement of the Bushveld Complex further to the north. The ferrobasaltic magma proposed to be parental to the LI-HI-RC bodies differs substantially from parental magmas (high-Mg andesite, or boninite?, and tholeiitic basalt; Sharpe 1981; Harmer and Sharpe, 1985; Hatton and Sharpe, 1989) proposed for the Bushveld Complex. It is well documented that most large igneous provinces, either continental or oceanic, have alkalic mafic rocks associated with them (BVSP, 1981), and the indication is that the HITIS fulfill this role relative to the voluminous Bushveld Complex. We may speculate that in the LI-HI-RC rocks we see the products of either a failed rift or a flanking rift relative to an active magmatic system to the north.

It is noted that the HITIS bodies in the Vredefort-Heidelberg area roughly follow a westerly trend parallel to the long axis of the Bushveld Complex. Also following the same direction, is the pre-Karoo, post-Ventersdorp fault system to the west of the Vredefort Dome, which has the Sugarbush Fault as a dominant feature. These faults show an early left-lateral horizontal wrench component and a late normal fault component (Pretorius, 1964; Myers *et al.*, 1987). Pretorius (1964) refers to a number of "Sugarbush-type" faults in this area and he described them as being normal faults having sinuous courses and with considerable displacements. Myers *et al.* (1987) argued for a single, early to syn-Witwatersrand, northeast to southwest compressional event to have initially caused left lateral shear along these faults, and, finally due to stress relief, yielded to extensional tectonics with the extrusion of the Klipriviersberg volcanics. However, Cluver (1957) earlier contended that although the horizontal movement on these faults is pre-Transvaal, the normal component post-dates the Transvaal rocks. We postulate that the normal faulting (half-grabens?) represented by the "Sugarbush-type" faults relates to the rifting event proposed in this paper. Traces of these faults to the west are largely obliterated by the Vredefort impact event and now largely covered by the Karoo sedimentary rocks.

An outline of events gleaned from the information supplied in this paper is given in Table 9 and Figure 16.

Conclusions

The Lindeques Drift (LI) and Heidelberg (HI) Intrusions and the volcanic Roodekraal Complex (RC) derive from a ferrobasaltic magma with alkaline affinities (MgO = 4.8 %, TiO_2 =1.8 percent, P_2O_5 = 0.52 percent, $Zr/(P_2O_5 \bullet 10^4)$ = 0.02, Nb/Y=1.47, K_2O/Yb =1.3, Ta/Yb = 1.1) that was emplaced as a number of km-sized mafic bodies to the north and northeast of the Vredefort impact structure, prior to impact. The ferrobasaltic magma, with low Al and high Fe contents, most probably results from deep-crustal amphibole(-plagioclase) fractionation of an alkali basaltic precursor in an embryonic continental rift setting that formed during the emplacement of the Bushveld Complex further to the north. Mild crustal contamination of the ferrobasaltic magma is indicated by enrichment patterns in the LIL elements. The dominant

rock types in the LI (zircon SHRIMP age: 2054.8±5.7 Ma) and HI are even-grained and porphyritic spessartite, representing clinopyroxene-magnetite(-ilmenite) ± olivine cumulates with variable fractions of the interstitial ferrobasaltic magma. Amphibole (edenite-magnesiohastingsite), responsible for the porphyritic texture of some of the spessartite, stabilized after clinopyroxene in paragenetic sequence, and its concentration is directly proportional to the amount of trapped liquid. The interstitial magma component also crystallized plagioclase, sphene, sulphide, apatite, microperthite and biotite. Discordant dykes and sills (?) of fine-grained diorite and syenodiorite, interpreted to be residual liquids of deeper but still shallow-level fractionation process, cut through the spessartite of the LI. Low-silica diorite with highly variable chemistry, crosscutting the LI spessartite, represents a desilicified and de-aluminated ferrobasaltic magma due to reaction with dolomite country rock. The RC (zircon SHRIMP age: 2053±9.2 Ma) formed contemporaneously with the LI and HI and is composed of hawaiite and mugearite lava flows and sub-flow diorite intrusions. The latter rocks are chemically hardly distinguishable from the diorite of LI and are believed to be co-genetic. A gabbro dyke, stratigraphically below and perpendicular to the LI, is provisionally not considered as a direct feeder to this intrusion. It might even be a younger intrusion unrelated to the LI.

Acknowledgements

Financial support by the Centre for Research on Magmatic Ore Deposits is gratefully acknowledged. We express our gratitude to Andries Bisschoff for introducing the first author to the LI and RC in the early 1980's; Anglo ED Africa for putting the drill cores of boreholes P31, OB1 and W1 at our disposal; Andreas Spath for the ICP-MS analyses done at UCT; Maggi Loubser and Peter Graeser for analytical work; and Rina White for drafting of the diagrams. We also thank Chris Hatton and an anonymous referee for useful contributions to improve the clarity of the paper.

References

Albat, H.M. and Mayer, J.J. (1989). Megascopic planar shock fractures in the Vredefort Structure: a potential time marker? *Tectonophysics*, **162**, 265-276.

Armstrong, R.A., Compston, W., Retief, E.A., Williams, I.S. and Welke, H.J. (1991). Zircon ion microprobe studies bearing on the age and evolution of the Witwatersrand triad. *Precambrian Research*, **53**, 243-266.

Arth, J.G., Arndt, N.T. and Naldrett, A.J. (1977). Genesis of Archean komatiites from Munro Township, Ontario: Trace element evidence. *Geology*, **5**, 590-594.

Bennett, H. and Oliver, G. (1992). XRF Analysis of Ceramics, Minerals and Applied Materials. *John Wiley and Sons, United Kingdom*, 298 pp.

Bisschoff, A.A. (1972). The dioritic rocks of the Vredefort dome. *Transactions of the Geological Society of South Africa*, **75**, 31-45.

Bisschoff, A.A. (1999). Vredefort Dome. Explanation of geological sheets 2627CA, CB, CC, CD, DA, DC and 2727AA, AB, BA (1:50000). *Council for Geoscience, South Africa*, 49pp.

Boon, J.D. and Albritton, J. (1936). Meteorite craters and their possible relationship to 'cryptovolcanic structures'. *Field and Laboratory*, **5**, 53-64.

Burger, A.J. and Coertze, F.J. (1975). Age determinations – April 1972 to March 1974. *Annals of the Geological Survey of South Africa*, **10**, 135-141.

BVSP (1981). Basaltic volcanism on terrestrial planets. Pergamon Press Inc, New York, United States of America, 1286pp.

Clark, R.J.McH. (1972). The geology of the Roodekraal Igneous Complex. Potchefstroom District. Unpublished MSc dissertation, University of the Witwatersrand, South Africa, 137pp.

Cluver, A.F. (1957). On the tectonic history and some related sedimentational aspects of the Witwatersrand System in the far east Rand, during upper Witwatersrand pre-Transvaal System time. *Annals of the University of Stellenbosch*, **33A.**, 71-124..

Cornell, D.H., Armstrong, R.A. and Walraven, F. (1998). Geochronology of the Proterozoic Hartley Basalt Formation, South Africa: constraints on Kheis tectogenesis and Kaapvaal craton's earliest Wilson cycle. *Journal of African Earth Sciences*, **26**, 5-27.

Cumming, G.L. and Richards, J.R. (1975). Ore lead isotope ratios in a continuously changing earth. *Earth and Planetary Science Letters*, **28**, 155-171.

De Waal, S.A. and Theart, H.F.J. (2004). Amphibole(-plagioclase) fractionation in the high-Ti parental magma of the Basal Gabbro Unit, Uitkomst Complex, and the implications for the associated sulphide mineralization. *Geoscience Africa 2004, Abstract Volume, Johannesburg, South Africa*, 160-161.

De Waal, S.A. and Armstrong, R.A. (2000). The age of the Marble Hall diorite, its relationship to the Uitkomst Complex, and evidence for a new magma type associated with the Bushveld magmatic episode. *South African Journal of Geology*, **103**, 128-140.

De Waal, S.A., Maier, W.D., Armstrong, R.A. and Gauert, C.D.K. (2001). The age and parental magma of the Uitkomst Complex. *Canadian Mineralogist*, **39**, 557-571.

Dietz, R.S. (1961). Vredefort ring structure: meteorite impact scar?, *Journal of Geology*, **69**, 499-516.

Floyd, P.A. and Winchester, J.A. (1975). Magma-type and tectonic setting discrimination using immobile elements. *Earth and Planetary Science Letters*, **27**, 211-218.

French, B.M. and Nielsen, R.L. (1990). Vredefort Bronzite Granophyre: chemical evidence for origin as a meteorite impact melt. *Tectonophysics*, 171, 119-138.

Frick, C. (1975). The geology and petrology of the Kaffirskraal igneous complex. *Transactions of the Geological Society of South Africa*, **78**, 11-23.

Frick, C. (1979). Geology, mineralogy and petrology of the Kaffirskraal Complex. *Geological Survey of South Africa Bulletin*, **64**, 42pp.

Green, T.H. (1982). Anatexis of mafic crust and high pressure crystallization of andesite. *In*: R. S. Thorpe (Editor), Andesites. *John Wiley and Sons, New York, U.S.A.*, 465-488.

Hargraves, R.B. (1961). Shatter cones in the rocks of the Vredefort Ring. *Transactions of the Geological Society of South Africa*, **64**, 147-161.

Harmer, R.E. and Sharpe, M.R. (1985). Field relations and strontium isotope systematics of the Marginal Rocks of the Eastern Bushveld Complex. *Economic Geology*, **80**, 813-837

Hatton, C.J. and Sharpe, M.R. (1989). Significance and origin of boninite-like rocks associated with the Bushveld Complex. *In:* A. J. Crawford (Editor), Boninites. *Unwin Hyman, London, United Kingdom*, 147-207.

Hess, P.C. (1989). Origins of rocks. *Harvard University Press, Cambridge, United States of America*, 336pp.

Jakobsson, S.P. (1979). Outline of the petrology of Iceland. *Jökull*, **29**, 57-73.

Jansen, H. (1954). The Losberg intrusive complex near Fochville, southern Transvaal. *Transactions of the Geological Society of South Africa*, **57**, 1-18.

Joesten, R. (1975) Mineralogical and chemical evolution of contaminated igneous rocks at a gabbro-limestone contact, Christmas Mountains, Big Bend region, Texas. *Geological Society of America Bulletin*, **88**, 1515-1529.

Kamo, S.L., Reimold, W.U., Krogh, T.E. and Colliston, W.P. (1996) A 2.023 Ga age for the Vredefort impact event and a first report of shock metamorphosed zircons in pseudotachylite breccias and granophyre. *Earth and Planetary Science Letters*, **144**, 369-388.

Larsen, L.M., Fitton, G.F. and Pedersen, A.K. (2003). Paleogene volcanic ash layers in the Danish basin: compositions and source areas in the North Atlantic igneous province. *Lithos*, **71**, 47-80.

Leake, B. E., Woolley, A. R., Birch, W. D., Burke, E. A.J., Ferraris, G., Grice, J. D., Hawthorne, F. C., Kisch, H. J., Krivovichev, V. G., Schumacher, J. C., Stephenson, N. C.N. and Whittaker, E. J.W. (2004). Nomenclature of amphiboles: Additions and revisions to the International Mineralogical Associations amphibole nomenclature. *American Mineralogist*, **89**, 883-887.

Le Bas, M.J. (1962). The role of aluminium in igneous clinopyroxene with relation to their parentage. *American Journal of Science*, **260**, 267-288.

Le Bas, M.J., Le Maitre, R.W., Streckeisen, A. and Zanettin, B. (1986). A chemical classification of volcanic rocks based on total alkali-silica diagram. *Journal of Petrology*, **27**, 745-750.

Le Maitre R.W. (1976). The chemical variability of some common igneous rocks. *Journal of Petrology*, **17**, 589-637.

Le Maitre, R.W. (Editor) (2002). Igneous rocks. A classification and glossary of terms. *Cambridge University Press, United Kingdom*, 236pp.

Ludwig, K.R. (1999). Isoplot/Ex version 2.00: A geochronological toolkit for Microsoft Excel. Berkeley Geochronology Centre, California, United States of America, Special publication 1a, 46pp.

Ludwig, K.R. (2000). SQUID 1.00: A User's Manual. *Berkeley Geochronology Centre, California, United States of America, Special Publication*, **2**, 17pp

Martini, J.E.J. (1978). Coesite and stishovite in the Vredefort Dome, South Africa. *Nature*, **272**, 715-717.

Martini, J.E.J. (1991). The nature, distribution and genesis of the coesite and stishovite associated with pseudotachylite of the Vredefort Dome, South Africa. *Earth and Planetary Science Letters*, **103**, 285-300.

McBirney, A.R. (1993). Igneous petrology. Second Edition. *Jones and Bartlett Publishers, Boston, United States of America*, 508pp.

Myers, M., Myers, R.E. and McCarthy, T.S. (1987). Re-examination of the Sugarbush Fault and associated structures. *South African Jounal of Geology*, **90**, 270-281.

Middlemost, E.A.K. (1989). Iron oxidation ratios, norms and the classification of volcanic rocks. *Chemical Geology*, **77**, 19-26.

Nel, L.T. and Jansen, H. (1957). The geology of the country around Vereeniging. *Geological Survey of South Africa, Explanation of the geological map sheet 62*, 90pp.

Nkouathio, D.G., Ménard, J.-J., Wandji, P. and Bardintzeff, J.-M. (2002). The Tombel graben (West Cameroon): a recent monogenetic volcanic field of the Cameroon line. *Journal of African Earth Sciences*, **35**, 285-300.

Paces, J.B., and Miller, J.D. (1989) Precise U-Pb ages of the Duluth Complex and related mafic intrusions, north-eastern Minnesota: geochronological insights to physical, petrogenic, palaeomagnetic and tectonmagmatic processes associated with the 1.1 Ga mid-continent rift system. *Journal of Geophysical Research*, **98B**, 13997-14013.

Pearce, J.A. (1982). Trace element characteristics of lavas from destructive plate boundaries. *In*: R. S. Thorpe (Editor), Andesites. *John Wiley and Sons, New York, U.S.A.*, 525-548.

Poujol, M., Anhaeusser, C.R. and Armstrong, R.C. (2002). Episodic granitoid emplacement in the Archaean Amalia-Kraaipan terrane, South Africa: confirmation from single U-Pb geochronology. *Journal of African Earth Sciences*, **33**, 435-449.

Poujol, M., Kiefer, R., Robb, L.J., Anhaeusser, C.R. and Armstrong, R.A. (2005). New U-Pb data on zircons from the Amalia greenstone belt Southern Africa: insights into the Neoarchaean evolution of the Kaapvaal Craton. *South African Journal of Geology*, **108**, 317-332.

Pretorius, D.A. (1964). Geology of the South Rand Basin. *In:* S. H. Houghton (Editor), The Geology Of Some Ore Deposits In Southern Africa. *Geological Society of South Africa*, 625 pp.

Reimold, W.U. and Gibson, R.L. (1996). Geology and evolution of the Vredefort Impact Structure, South Africa. *Journal of African Earth Sciences*, **23** 125-162.

Rollinson, H. (1993). Using geochemical data: evaluation, presentation, interpretation. *Harlow, Essex, England, Longman Scientific and Technical*. 352pp.

Sharpe, M.R. (1981). The chronology of magma influxes to the eastern compartment, Bushveld Complex, as exemplified by its marginal border groups. *Journal of the Geological Society London*, **138**, 307-326.

Schmitz, M.D. and Bowring, S.A. (2002). The significance of the U-Pb zircon dates in lower crustal xenoliths from the southwestern margin of the Kaapvaal Craton, southern Africa. *Chemical Geology*, **172**, 59-76.

Taylor, S.R. and McLennan, S.M. (1985). The continental crust: its composition and evolution. *Oxford, Blackwell Scientific Publications, United Kingdom*, 312pp.

Thompson, R.N. (1982). British tertiary volcanic province. *Scottish Journal of Geology*, **18**, 49-107.

Thompson, R.N., Morrison, M.A., Dickin, A.P. and Hendry, G.L. (1983). Continental flood basalts ... Arachnids rule OK? *In*: C. J. Hawkesworth and M. J. Norry (Editors) Continental basalts and mantle xenoliths. Nantwich, Shiva Publishing, United Kingdom, 158-185.

Walraven, F. (1997). Gechronology of the Rooiberg Group, Transvaal Supergroup, South Africa., *Economic Geology Research Unit Information circular, University of the Witwatersrand, South Africa*, **316**, 21pp.

Walraven, F. and Hattingh, E. (1993). Geochronology of the Nebo Granite, Bushveld Complex. *South African Journal of Geology*, **96**, 31 – 41.

Walraven, F. and Martini, J. (1995). Zircon Pb-evaporation age determinations of the Oak Tree Formation, Chuniespoort Group, Transvaal Sequence: implications for Transvaal-Griqualand West basin correlations. *South African Journal of Geology*, **98**, 58-67.

Watson, J.S. (1996). Fast, simple method of powder pellet preparation for X-Ray fluorescence analysis. *X-Ray Spectrometry*, **25,** 173-174.

Williams, I.S. (1998). U-Th-Pb geochronology by ion microprobe. *In*: M. A. McKibben, W. C. Shanks III and W. I. Ridley (Editors), Applications of microanalytical techniques to understanding mineralizing processes. *Reviews in Economic Geology*, **7**, 1-35.

Wyllie, P.J. (1974). Limestone assimilation. *In*: H. Sorensen (Editor), Alkaline rocks. *John Wiley and Sons, New York, United States of America*, 459-474.

Editorial handling: J. M. Barton Jr.

Appendix I : Methods of investigation

Thin and polished thin sections were investigated with an optical microscope. Selected grains of clinopyroxene, plagioclase, amphibole and biotite were analysed on a Cameca SX100 electron microprobe at the Department of Geology, University of Pretoria. Counting times on peak positions were 20 seconds, and 10 seconds on each background position. The electron beam was defocused to a 10-micron diameter for feldspar. Wollastonite was used as standard for Si and Ca, pure oxides for Mg, Al, Mn, Cr, Ti, Ni, and Fe, orthoclase for K, albite for Na, tugtupite for Cl, and fluorite for F. A ZAF corrections procedure was applied throughout.

Selected samples were analyzed for major and trace elements on an ARL 8420 wavelength-dispersive XRF spectrometer in the XRF/XRD Laboratory of the Department of Geology, University of Pretoria. Samples were dried and roasted at 950°C to determine percentage loss on ignition (LOI). Major-element analyses were performed on fused discs, following a standard method adapted from Bennett and Oliver (1992). One gram of pre-roasted sample is mixed with 6 g lithium tetraborate flux in a 5 % Au/Pt crucible, and fused at 1050°C in a muffle furnace with occasional swirling. Glass disks were poured into a pre-heated Pt/Au mould, with the bottom surface presented for analysis. The samples were analyzed for selected trace elements on pressed powder pellets with saturated Movial solution as binder, using an adaptation of the method described by Watson (1996). The XRF spectrometer was calibrated with certified reference materials. The NBSGSC fundamental parameter program was used for matrix correction for the major elements as well as of Cl, Co, Cr, V, Ba and Sc. The Rh Compton peak ratio method was used for the other trace elements.

Rare Earth and selected trace elements were analyzed at the Department of Earth Sciences, University of Cape Town. 50-mg sample aliquots were dissolved by a standard acid digestion procedure using ultra-clean HF and HNO_3. Calibration was made using external synthetic multi-element standards. The samples were then analyzed using a Perkin Elmer / Sciex Elan 6000 ICP-MS. Internal standardization was achieved using 103Rh, 115In, 187Re and 209Bi. Typical detection limits for all the rare earth elements are in the ppt range. Each sample solution was analyzed in triplicate, with 20 sweeps per replicate, and the data quoted represent average values of these triplicate analyses. Both the within-run and duplicate analysis precision was mostly between 2% relative and always better than 3% relative (1 sigma).

Zircons were separated at the University of Pretoria (X743) and the Research School of Earth Sciences (RSES), Canberra (X386P). The grains were mounted in epoxy resin at RSES, polished and then photographed in reflected and transmitted light. These images together with those obtained under a scanning electron microscope fitted with cathodoluminescence imaging apparatus were used to provide information on zonation, and occurrence/absence of inherited cores, metamorphic overgrowths and alteration. The least altered zircon grains were then analysed using the SHRIMP II spectrometer during a single session. Each analysis consisted of 6 scans through the mass range. The SHRIMP data were then reduced in a manner similar to that of Williams (1998, and references therein) using the SQUID Excel Macro of Ludwig (2000). U/Pb in the unknowns were normalised to a $^{206}Pb/^{238}U$ value of 0.1859 (equivalent to an age of 1099.1 Ma) for standard AS3 (Paces and Miller, 1989). The U and Th concentrations were determined relative to those measured in the SL13 standard. Ages were calculated using the radiogenic $^{207}Pb/^{206}Pb$ ratios, with the correction for common Pb made using the measured ^{204}Pb and the appropriate common Pb composition, assuming the model of Cumming and Richards (1975). Uncertainties in the isotopic ratios and ages are reported in the 1s level unless otherwise stated in the text, and the final weighted mean ages are reported as 95% confidence limits. The Concordia plots and weighted mean age calculations were carried out using Isoplot/Ex (Ludwig, 1999).

Least squares optimization was used to evaluate possible mixing models for the spessartite. The function minimized is:

$$*[(A_i X_{i,j}) - Y_{i,j}]2$$

where A_i refers to the fraction of the i^{th} phase in the mineral mixture, $X_{i,j}$ and $Y_{i,j}$ refer to concentration of the j^{th} element oxide in the i^{th} phase in the minerals and interstitial magma making up the cumulus mush, and spessartite representing the mineral mixture, respectively. The feasibility of the different models were judged by the arbitrary function:

feasibility index = sq. rt. [abs (plag) •MSD].

This function is based on the arguments that plagioclase concentrations in the cumulus mixture should be close to zero as required by the almost complete absence of negative Eu anomalies in the residual lava/diorite, and MSD, which is the mean of the square of the deviations, Y_j(observed)-Y_j (calculated), shows the "goodness of fit" of the model and ideally should also be zero. Minor deviations (< ~ 5%) of the calculated concentrations above or below zero may be statistically insignificant considering local variations in mineral chemistry.

A full set of all calculations is available from the corresponding author, and only one example is given below (Table A1). All compositions are volatile-free and recalculated to a total of 100. Numbers in bold are allowed to vary in the least squares optimization calculation. No constraints on the model were introduced. Calcspess represents calculated data and Pspess the observed data (whole rock composition). SD is the square of the deviation and SSD is the sum of these squares.

Table A1. Cumulate model for LI porphyritic spessartite
Interstitial magma : RC lava

	Cpx	Mt	Plag	Magma	Olivine	Dolomite	Calcspes	Pspess	Diff.	SD
Fraction ->	**0.34**	**0.20**	**0.06**	**0.30**	**0.04**	0.05	1.00			
SiO_2	51.39	0.00	59.65	55.05	36.31	0.00	39.71	39.69	0.0	0.00
TiO_2	0.55	12.46	0.00	1.81	0.11	0.00	3.24	3.23	0.0	0.00
Al_2O_3	1.56	0.00	25.11	12.66	0.13	0.00	5.98	5.99	0.0	0.00
Fe_2O_3T	12.02	87.54	0.71	13.27	28.36	0.00	27.01	26.99	0.0	0.00
MnO	0.39	0.00	0.00	0.19	0.48	0.00	0.21	0.31	0.1	0.01
MgO	11.73	0.00	0.00	3.44	34.51	42.00	8.47	8.45	0.0	0.00
CaO	21.56	0.00	6.50	5.61	0.13	58.00	12.18	12.16	0.0	0.00
Na_2O	0.80	0.00	7.80	5.61	0.08	0.00	2.47	2.34	-0.1	0.02
K_2O	0.01	0.00	0.48	1.66	0.05	0.00	0.54	0.61	0.1	0.00
P_2O_5	0.00	0.00	0.00	0.53	0.00	0.00	0.16	0.24	0.1	0.01
Fraction Fe_2O_3 in Mt(-ilm) =	**0.88**			Fraction TiO_2 in Mt(-ilm) =		0.12				
									SSD =	0.04